THE PENNSYLVANIA STATE UNIVERSITY
SCHREYER HONORS COLLEGE

DEPARTMENT OF CHEMISTRY

SYNTHESIS AND CHEMICAL CONVERSION OF METAL AND BINARY INTERMETALLIC NANOPARTICLES

MATTHEW DWIGHT STRAESSER
SPRING 2011

A thesis
Submitted in partial fulfillment
of the requirements
for a baccalaureate degree
in Chemistry
with honors in Chemistry

Reviewed and approved* by the following

Raymond E. Schaak
Associate Professor of Chemistry
Thesis Supervisor

Kenneth S. Feldman
Professor of Chemistry
Honors Advisor

Mary Elizabeth Williams
Associate Professor of Chemistry
Faculty Reader

*Signatures are on file in the Schreyer Honors College

ABSTRACT

The synthesis and chemical oxidation of metal and binary intermetallic nanoparticles was studied. Specifically, the syntheses of Ni_3Sn_4 and Bi_3Ni were successfully conducted using edible plant and seed oils. A solvent recyclability study of safflower oil was also conducted using the Ni_3Sn_4 system. Sodium nitrite ($NaNO_2$) was used to fully oxidize metal nanoparticles of Pb, Sn, and In and partially oxidize Bi and Te; generally, the particle morphology was retained during the oxidation. Powder XRD and TEM confirmed the successful oxidations. β-In_3Sn was then oxidized with $NaNO_2$ to yield indium tin oxide nanoparticles. Again, the particle's morphology was maintained throughout the oxidation. Powder XRD, SEM, and TEM confirmed the successful oxidation of β-In_3Sn to indium tin oxide.

TABLE OF CONTENTS

LIST OF FIGURES

LIST OF TABLES

ACKNOWLEDGEMENTS

First, I would like to thank Dr. Raymond Schaak for giving me the opportunity to conduct research in his laboratory. His support and advising has been of incalculable worth since I joined the group.

It is likely that I wouldn't have accomplished this work without the support and advice of Nathaniel Henderson, Nam Chou, and Mary Elizabeth Anderson. For the aforementioned individuals, thank you for taking me under your wings and teaching me the ropes of chemistry. I would also like to thank all the other members of the Schaak group: all of whom have helped me at one point or another and I am very grateful.

Although I am the only titled author of this thesis, it was truly a collaborative effort and I could not have accomplished it without the help of the aforementioned individuals.

Last but certainly not least, I would like to thank the One who created me, brought me life, and bestowed every blessing upon me in this world. I would also like to thank my family for their support, inspiration, and determination they gave me throughout all of college.

Chapter 1

Introduction: Background, Green Metallurgy, Nitrite Oxidation, Indium Tin Oxide

1.1 Background

Solution-mediated metallurgy is a relatively recent area of chemistry which has received significant attention. The concept of synthesizing metallurgical solids with a solution-mediated process was first dubbed "metallurgy in a beaker" by the Schaak group.[1] Here, metals and metallurgical solids, normally obtained by harsh reaction conditions, were accessed using solution-mediated routes. Traditionally, metals and metallurgical solids, such as intermetallic compounds, are synthesized using harsh reaction conditions such as furnace annealing and arc melting. These traditional reactions are not only time and energy intensive but they often lead to significant product loss. By using solution-mediated processes, these same metallurgical solids can be obtained in a much less costly manner and with high product yield. Using solution-mediated routes, nanoparticles can (in addition to bulk-scale solids) also be obtained readily. Traditionally, nanoparticles are generated using ball milling[2] and then mesh filtering. This method generates polydisperse particle size distributions and completely lacks morphology control. However, solution-mediated processes can generate uniform particle morphologies and isotropic sizes.[3] Morphology control lends a significant advantage to solution-mediated reactions over traditional routes.

Metals made using "beaker chemistry" are generally synthesized by starting with the metal salt. The metal salt is either thermally reduced by the solvent or by injection of a reducing agent, commonly $NaBH_4$.[4] The reduction of metal salts to M^0 generates metal nanoparticle seeds which rapidly combine with one another to form the nanoparticles. The growth of the nanoparticles can be controlled using a variety of factors. One such a factor is the reduction

kinetics.[5] The kinetics are varied by either the rate of addition of the reducing agent or by the reduction temperature of the solvent, if being thermally reduced by the solvent. The control of the reduction kinetics can lead to the control of the growths of the crystal planes. This leads directly to the shape-controlled synthesis of metal nanoparticles.[5]

Solution-mediated chemical conversions of metals used to expand the types of materials accessible as nanoparticles, are conducted using various routes. For example, binary intermetallic compounds are synthesized by reacting a molten metal with another non-molten reagent. In this reaction, the molten metal diffuses into the non-molten metal and forms the intermetallic compound.[6] Another type of chemical conversion is oxidation reactions. Oxidation reactions are usually carried out in solution by using a chemical oxidizing agent[7] such as bubbling oxygen into the solution at elevated temperatures.[8] For example, iron oxide nanoparticles are commonly synthesized by bubbling air into the colloidal, iron nanoparticle solution at elevated temperatures.[8] Similar to oxidation reactions are the reactions of metals with other chalcogenides to form semiconductors. For example, PbS nanoparticles, a known semiconductor frequently used as an infrared detector,[9] are often synthesized by reacting pre-synthesized Pb nanoparticles with elemental sulfur.[10] In all types of solution-mediated chemical conversion reactions, a clear advantage to the traditional route, besides less costly and energy intensive conditions, is the preservation of the nanoparticle morphology, which is often destroyed using traditional routes.

The scope of this work is by no means exhaustive. The work presented here focuses on the shape-controlled synthesis and chemical conversion of metal and binary intermetallic nanoparticles. More specifically, the conversion of two metals to binary intermetallics

synthesized *via* molten diffusion of one of the metal constituents and the shape-controlled chemical oxidation of metals and intermetallic systems was explored.

1.2 Green Metallurgy

With the recent establishment of the principles of green chemistry, there has been a significant push to develop environmentally-responsible chemical transformations.[11] Most of the work has been on bulk-scale organic reactions due to their industrial and technological relevance. However, there is a growing interest in the area of green nanotechnology, which includes the use of nanoscale materials for catalysis and environmental remediation, and the development of green synthetic routes for nanoscale materials.[12] One such example involves the use of edible oils to synthesize a variety of nanocrystalline materials, including semiconductors.[13] A similar area, which has received less attention, is the development of bulk-scale metallurgical synthetic routes that incorporate the principles of green chemistry. Traditional bulk-scale metallurgy usually requires harsh reaction condition such as arc melting and furnace annealing; however, the Schaak group has shown that these conditions can be avoided by utilizing molten metal diffusion in a polyol solvent, where the solvent serves as a heat source and a dispersion media.[14] In these reactions, the system is heated to above the melting point of one the constituent metals and the molten metal forms a colloidal solution. The molten metal then attacks the other crystalline metal and it diffuses into the crystalline metal's lattice, forming an intermetallic. Extending from this work, here a more environmentally-responsible bulk-scale synthesis of Bi_3Ni and Ni_3Sn_4 using edible plant and seed oils is presented.

The solution mediated bulk-scale synthesis of intermetallics is accomplished by reacting the constituents in a high boiling solvent, typically tetraethlyene glycol. In this route, the

reaction solution is heated to above the melting point of one of metal constituents and then held at that temperature until the diffusion has taken place. One limitation to this method is that one of the metal constituents must melt below the boiling point of the solvent, which in the case of tetraethlyene glycol is 300 °C. It seems feasible that a substitution from the toxic tetraethlyene glycol to a more environmentally-responsible solvent, such as edible plant and seed oils, would be a reasonable goal, considering that the solvent primarily serves as a heat source and a dispersion media. However, several challenges emerge. The smoke points of most plant and seed oils are considerably lower than the boiling point of tetraethlyene glycol, 300 °C. For example, apricot kernel oil has a smoke point of 257 °C. This potentially limits the use of metals such as bismuth, m.p. 271 °C. Also, it is well known that long chain fatty acids, such as oleic and linoleic acid which are both major components of plant and seed oils, can serve as surface surfactants. This is due to the carboxylic acids adhering strongly to the metal or metal oxide surfaces. In such instances, it has been shown that the surfactant slows the diffusion rate due to surface passivation. This is not an issue in polyol solvents because the alcohols do not adhere to the metal or metal oxide surfaces.

1.3 Nitrite Oxidation

Metal oxides are traditionally synthesized by reacting the zero valent metal(s) at extremely high-temperatures with oxygen. One example of this type of reaction is furnace annealing.[15,16] However, this technique generates oxides with no morphology control and requires harsh, high-temperature conditions. An area that has received less attention is solution-mediated nanoparticle oxidation.[17,18] The key advantage of solution-mediated oxidations is that the nanoparticle's morphology can be preserved during the reaction. Work pertaining to solution-mediated metal nanoparticle oxidation has primarily been focused on using oxygen as

the oxidizing agent.[19] For example, air is commonly used to oxidize iron nanoparticles to iron oxide nanoparticles. Despite the known utility of common organic and inorganic oxidizing agents, there has been very limited research conducted on the use of such oxidizing agents applied to solution-mediated, nanoparticle oxidation. There are several advantages of using a chemical oxidizing agent as opposed to using air or the traditional methods. One such advantage is the reaction time. Using a chemical oxidizer usually allows for much faster reaction times by comparison to overnight heating in air. Another advantage to using chemical oxidizing agents is retention of the particle morphology. Traditional oxidizing methods usually destroy the particle morphology and thus become a disadvantage of this technique relative to chemical oxidizing methods.

Sodium nitrite has long been known to oxidize amines into amine compounds. In an acidic media, the amines are converted to diazonium ions.[20] The synthetic utility of the diazonium ion is to serve as a more facile leaving group in an S_N2 substitution. In organic synthesis, sodium nitrite is also used to destroy azides.[21] By comparison, potassium permanganate and chromic acid are commonly used to oxidize alcohols to ketones and carboxylic acids.[22] Potassium permanganate also has been known to cleave alkenes into ketones and aldehydes.[22] Sodium nitrite is by no means as strong as an oxidizer as potassium permanganate and chromic acid: the presence of alcohols and alkenes from either the surface stabilizer or the solvent renders strong oxidizing agents useless. Despite the known oxidizing strength of sodium nitrite, there are no reports of it being used to oxidize metal nanoparticles.

There are several advantages ascertained by using sodium nitrite as a chemical oxidizing agent. Sodium nitrite is highly soluble in polar media (solubility in water = 82 g mL^{-1}).[23] This relatively high solubility makes the dissolution of sodium nitrite into organic polar media, such

as polyols and dimethyl sulfoxide, feasible. Also, sodium nitrite has a relatively high thermal stability by comparison to other oxidizing agents. For example, sodium nitrite, chromium trioxide, potassium permanganate, and osmium tetroxide have decomposition temperatures of 271, 251, 240, and 130 °C.[23-26] The decomposition temperatures imply that sodium nitrite can be heated to higher temperatures without decomposition. Sodium nitrite's toxicity is also significantly lower than the other chemical oxidizers in its class. In fact, sodium nitrite commonly serves as a vasodilator in medical applications as well as a curing and preserving agent in the food industry.[27]

The chemical oxidation of metal nanoparticles was accomplished by dissolving the sodium nitrite in a high boiling polyol or non-reducing dimethyl sulfoxide solvent. The sodium nitrite solution was subsequently added to a dispersion of either Te, Bi, Sn, In, or Pb metal nanoparticles. There are some limitations to this oxidizing method. One limitation associated with using dimethyl sulfoxide is the reaction temperature, limited by the solvent's boiling point (189 °C). On the other hand, using a high boiling solvent such as tetraethlyene glycol allows the reaction to be heated to 300 °C; however, the reducing strength of the glycol becomes significantly stronger as the temperature is raised and thus the reducing action of the solvent may counteract the oxidizing strength of the sodium nitrite.

1.4 Indium Tin Oxide

Tin doped indium oxide (ITO) has received significant attention recently due to its unique properties such as optical transparency, electrical conductivity, and its wide, composition dependent band-gap (1.38-4.14 eV).[28] These properties have yielded extensive applications in consumer electronics and as a transparent, conducting film in photovoltaic energy conversion.[29]

In consumer products and solar cells, ITO is typically applied as a thin film. Traditional thin film deposition techniques include vacuum arc plasma evaporation, furnace evaporation/oxidation, magnetron sputtering, and molecular beam epitaxy.[30-33] Clearly, these methods are energy and cost intensive, requiring expensive apparati, and can lead to significant product loss, which is non-trivial considering the current price of indium. An alternative synthetic and deposition method would be to utilize solution-mediated reactions to obtain the ITO nanoparticles, which could then be drop-casted as a thin film. Recent work has yielded solution-mediated ITO nanoparticle routes. These routes typically utilize the thermal decomposition of the In and Sn precursors in non-polar media, the alkaline hydrolysis of the In and Sn precursors, or the co-precipitation of $In(OH)_3$ and $Sn(OH)_4$ to yield to ITO particles.[34-38]

Another route, of which there are few reports, is to synthesize an In-Sn alloy[39] or the β-In_3Sn intermetallic nanoparticles and oxidize them to ITO, which is reported here. The synthesis is achieved by first synthesizing the β-In_3Sn, made by diffusing molten In metal into pre-synthesized β-Sn particles, and then chemically oxidizing the β-In_3Sn to ITO using sodium nitrite. There are several potential advantages to this method. One potential advantage is Sn variance of the ITO particles. The β-In_3Sn intermetallic phase has a natural variance of 12-44 percent Sn. Thus, the subsequent oxidation of the β-In_3Sn particles would have a potential Sn variability of 12-44 percent.[40] The Sn variability would affect the physical properties of the ITO particles; the band-gap would decrease and the electrical conductivity would increase as the Sn content is increased. The Sn variability could lead to band-gap control. Another advantage is that the entire synthesis route can be accomplished at relatively low temperatures, less than 180 °C. However, there are several disadvantages encountered using this synthetic route. The primary disadvantage is that In metal melts (m.p. = 157 °C) at a higher temperature than the β-

In_3Sn (m.p. = 150 °C).[40] This causes the diffusion process to yield liquid particles. The liquid particles quickly combine with one another to produce larger particles and thus the shape and size control of the nanoparticles becomes difficult. Although addition of a surface stabilizer reduces the particle-particle interactions, it still does not lead to facile shape and size control.

1.5 References

1. Schaak, R. E.; Sra, A. K.; Leonard, B. M.; Cable, R. E.; Bauer, J. C.; Han, Y. F.; Means, J.; Teizer, W.; Vasquez, Y.; Funck, E. S. *J. Am. Chem. Soc.* **2005,** *127*, 3506-3515.

2. Koch, C. C.; Whittenberger, J. D. *Intermetallics* **1996,** *4*, 339.

3. Yin, Y.; Alivisatos, A. P. *Nat.* **2005,** *437*, 664-670.

4. Chou, N. H.; Schaak, R. E. *J. Am. Chem. Soc.* **2007,** *129*, 7339-7345.

5. Chou, N. H.; Ke, X.; Schiffer, P.; Schaak, R. E. *J. Am. Chem. Soc.* **2008,** *130*, 8140-8141.

6. Henderson, N. L.; Schaak, R. E. *Chem. Mater.* **2008,** *20*, 3212-3217.

7. Peng, P.; Wang, C.; Xie, J.; Sun, S. *J. Am. Chem. Soc.* **2006,** *128*, 10676-10677.

8. Woo, K.; Hong, J.; Choi, S.; Lee, H. W.; Ahn, J. P.; Kim, C. S.; Lee, S. W. *Chem. Mater.* **2004,** *16*, 2814-2818.

9. Mcdonald, S. A.; Konstantatos, G.; Zhang, S.; Cyr, P. W.; Klem, E. J. D.; Levina, L.; Sargent, E. H. *Nat. Mater.* **2005,** *4*, 138-142.

10. Wang, Y.; Cai, L.; Xia, Y. *Adv. Mater.* **2005,** *17*, 473-477.

11. Anastas, P. T.; Warner, J. C. *Green Chemistry; Theory and Practice.* Oxford University Press, Oxford, **1998,** *30*. Poliakoff, M.; License, P. *Nat.* **2007,** *450*, 810. Noyori, R. *Chem. Commum.* **2005,** 1807.

12. Mao, Y.; Park, T. J.; Zhang, F.; Zhou, H.; Wong, S. S. *Small.* **2007,** *3*, 1122. Murphy, C. J. *J.Mater. Chem.* **2008,** *18*, 2173.

13. Raveendran, P.; Fu, J.; Wallen, S. L. *Green Chem.* **2006,** *8*, 34. Koltypin, Y.; Perkas, N.; Gedanken, A. *J. Mater. Chem.* **2004,** *14*, 2975. Spear, S. K.; Griffin, S. T.; Granger, K.S.; Huddleston, J. G.; Rogers, R. D. *Green Chem.* **2007,** *9*, 1008.

14. Henderson, N. L.; Schaak, R. E. *Chem. Mater.* **2008,** *20*, 3212.

15. Lee, J.; Sim, S.; Kim, K.; Cho, K.; Kim, S. *Mater. Sci. Engr. B.* **2005,** *122*, 85-89.

16. Leite, E.; Maciel, A.; Weber, I.; Lisboa-Filho, P.; Longo, E.; Paiva-Santos, C.; Andrade, A.; Pakoscimas, A.; Maniette, Y.; Schreiner, W. *Adv. Mater.* **2002,** *14,* 905-908.

17. Wang, W.; Yao, J. *J. Phys. Chem. C.* **2009,** *113,* 3070-3075.

18. Sarka, A.; Chadha, R.; Mukherjee, T.; Kapoor, S. *Chem. Phys. Lett.* **2009,** *473,* 111-115.

19. Cohen, T.; Dietz, A.; Miser, J. *J. Org. Chem.* **1977,** *42,* 2053-2058.

20. The National Academies Press, Prudent Practices in the Laboratory: Handling and Disposal of Chemicals. 7.D.3.3 Metal Azides. http://books.nap.edu/openbook.php?record_id=4911&page=165 (accessed March 11, 2011).

21. McMurry, J. *Organic Chemistry*, 7th ed.; Thompson: Belmont, CA, 2008; p 237, 624-625.

22. *Sodium Nitrite;* Material Safety and Data Sheet No. 563218; Sigma Aldrich: St. Louis, Missouri, (Feb 4) 2011, http://www.sigmaaldrich.com/catalog/DisplayMSDSContent.do (accessed March 11, 2011).

23. *Sodium Nitrate;* Material Safety and Data Sheet No. S5506; Sigma Aldrich: St. Louis, Missouri, (June 6) 2010, http://www.sigmaaldrich.com/catalog/DisplayMSDSContent.do (accessed March 11, 2011).

24. *Chromium Trioxide;* Material Safety and Data Sheet No. 27081; Sigma Aldrich: St. Louis, Missouri, (Mar 25) 2010, http://www.sigmaaldrich.com/catalog/DisplayMSDSContent.do (accessed March 11, 2011).

25. *Potassium Permanganate;* Material Safety and Data Sheet No. P2097; Sigma Aldrich: St. Louis, Missouri, (Dec 30) 2010, http://www.sigmaaldrich.com/catalog/DisplayMSDSContent.do (accessed March 11, 2011).

26. *Osmium Tetroxide;* Material Safety and Data Sheet No. O5500; Sigma Aldrich: St. Louis, Missouri, (Mar 13) 2010, http://www.sigmaaldrich.com/catalog/DisplayMSDSContent.do (accessed March 11, 2011).

27. Ghanbari, H. Hot dog preservative could be disease cure. *USA Today* [Online] **2005**, http://www.usatoday.com/news/health/2005-09-05-hot-dog-drug_x.htm (accessed Mar 11, 2011).

28. Gupta, L.; Mansingh, A.; Srivastava, P. *Thin Solid Films* **1989,** *176,* 33-44.

29. Kim, K.; Park, S. *Mater. Chem. Phys.* **2004,** *86,* 210-221.

30. Minami, T.; Ida, S.; Miyata, T. *Thin Solid Films* **2002,** *416,* 92-96.

31. Balasubramanian, N.; Subrahmanyam, A. *J. Phys. D: Appl. Phys.* **1989,** *22,* 206-209.

32. Meng, L.; dos Santo, M. *Thin Solid Films* **1998,** *322,* 56-62.

33. Dwyer, C.; Szachowicz, M.; Visimberga, g.; Lavayen, V.; Newcomb, S.; Sotomayor Torres, M. *Nat. Nanotechnol.* **2009,** *4,* 239-244.

34. Kim, H.; Kim, M.; Ha, Y.; Kanatizids, M.; Marks, T.; Facchetti, A. *J. Am. Chem. Soc.* **2009,** *131,* 10826-10827.

35. Park, Y.; Seo, K.; Lee, J.; Kim, J.; Cho, S.; O'Conner, C.; Lee, J. *J. Electroceram.* **2004,** *13,* 851-855.

36. Paramanik, N.; Biswas, P. *Bull. Mater. Sci.* **2002,** *6,* 505-507.

37. Saski, T.; Endo, Y.; Nakaya, M.; Kanie, K.; Nagatomi, A.; Tanoue, K.; Nakamura, R.; Muramatsu, A. *J. Mater. Chem.* **2010,** *20,* 8153-8157.

38. Kanehara, M.; Koike, H.; Yoshinaga, T.; Teranishi, T. *J. Am. Chem. Soc.* **2009,** *131,* 17736-17737.

39. Zhenguo, C.; Wang, C.; Zhao, L.; Zhou, Q. *Mater. Lett.* **2006,** *60,* 3096-3099.

40. *Phase Diagrams for Binary Alloys.* Okamoto, H.; ASM International: Materials Park, OH, 2000; p 491.

Chapter 2

Green Metallurgy: Bulk-Scale Intermetallic Synthesis

2.1 Introduction:

Green chemistry principles have been established to promote environmentally-responsible and non-hazardous routes for the synthesis of chemicals.[1] Towards that goal, a significant focus has been placed on modifying the chemistry of organic transformations, with emphasis on industrially relevant processes because of their scale and technological importance. There is also a growing interest in green nanotechnology, which includes the use of nanoscale materials for catalysis and environmental remediation, and novel synthetic routes to nanoscale solids.[2] For example, edible oils, which are non-toxic and renewable, have been used as solvents for the synthesis of a variety of nanocrystalline materials.[3] A similar area, which has received less attention, is the development of green bulk-scale solid synthesis methods of which are normally prepared by lengthy high-temperature solid-state reactions. Examples of ways in which green chemistry principles have been employed in bulk-scale solid state synthesis include the use of supercritical fluids and microwave heating.[4-5]

Metallurgical solids, including alloys and intermetallics, are typically synthesized using high-temperatures and harsh conditions. Such methods include high-temperature arc melting of the constituent elements and powder metallurgy techniques that involve heating the physical metal mixtures at high temperature, for long time periods, typically several days. These methods are both energy and thermally intensive, a direct consequence of the long solid-solid diffusion distances which must be overcome for the reaction to occur. Lower-temperature and lower-energy alternatives to the traditional methods include ball milling,[6] mechanochemical synthesis,[7] flux synthesis,[8] and various deposition techniques.[9]

Recently, solution chemistry techniques have proven to be applicable to the synthesis of nanoscale intermetallic compounds and alloys. For example, modifications of the polyol process and related methods have generated a library of late transition metal intermetallics and alloys.[10] To achieve the synthesis, metal salts are first dissolved in a high-boiling organic solvent (*e.g.* ethylene glycol and tetraethylene glycol): by heating, reduced *via* the solvent to zero-valent metals or by reduction with sodium borohydride prior to heating. The Schaak group has shown that a related strategy can be applied to the synthesis of bulk-scale intermetallic compounds. In this case, bulk elemental powders are heated in tetraethylene glycol and the powders diffuse together to form intermetallic phases.[11] This technique employs the molten diffusion of one of the constituents into the other. Molten diffusion works for metals which melt below the boiling point of the solvent, *e.g.* Sn and Bi. Here, the solvent serves as both a heat source, aiding the melting of the metal, and a dispersion medium. Utilizing this method, fourteen distinct bulk-scale intermetallic phases were synthesized at temperatures below 300 °C.[11]

By superimposing the principles of green chemistry on the inherently low-temperature solution technique for the synthesis of bulk-scale metallurgical solids, a more environmentally-responsible process becomes feasible. Since the solvent mainly serves as a heat source and dispersion medium, other non-toxic and renewable solvents become reasonable substitutions. Accordingly, it is shown that edible oils, which have been used previously to synthesize metal and semiconductor nanocrystals,[3] can serve as a reaction medium for the low-temperature synthesis of bulk-scale intermetallic compounds. More particularly, apricot kernel and safflower oils have been used to synthesize Bi_3Ni and Ni_3Sn_4, which have known applications as magnetic materials and battery electrodes. From a green chemistry stand point, this alternative metallurgy process yields increased energy efficiency, based on both lower temperatures and shorter

reaction times as compared to the traditional high-temperature synthetic methods, such as arc melting and powder metallurgy. This process also utilizes renewable oils and more environmentally-responsible reaction conditions compared to the typical solvents toxic glycols.[11]

2.2 Experimental

2.2.1 Materials

The following chemicals were used and purchased without further purification: Bi (99.5%) and Sn (99.8%) powders (-325 mesh, Alfa Aesar); Ni powder (-325 mesh, 99.8%, Alfa Aesar; 2-3 μm, 99%, Alfa Aesar). Apricot kernel and safflower oils were obtained from Spectrum Organics and used as purchased.

2.2.2 Synthesis

Bi_3Ni and Ni_3Sn_4 were both synthesized by placing stoichiometric amounts of the two constituent metals (approximate total mass of 0.15 g) into a flask with 30-50 mL of the respective oil. The system was purged with Ar, rapidly heated (~5-10 °C min^{-1}) with vigorous, continuous stirring (800-1150 rpm), and then held at the specific reaction temperature (Table 2-1) until the desired intermetallic phases were formed. The crystalline intermetallic powders were separated from the solvent *via* centrifugation, rinsed twice with toluene and then ethanol. Alternatively, all washings can be carried out in ethanol with additional rinsing. It was observed that lower stirring speeds or higher solvent viscosity can lead to attractions between the magnetic transition metal and the stir bar, which can cause local stoichiometry imbalances. Consequently, a slight excess (generally less than 5%) of metal remained; however, it can be easily removed by etching with ~2 M HCl prior to the final ethanol rinse. The formation of intermetallic phases was generally detectable by powder X-ray diffraction (XRD) within three hours of heating, but

longer heating times were necessary for phase-pure formation, consistent with a molten diffusion-based process. The synthetic parameters for the two phases are given in Table 2-1. Ni_3Sn_4 was studied further in order to investigate the solvent's recyclability. Ni_3Sn_4 was synthesized repeatedly in safflower oil, using the recovered solvent for subsequent reactions.

Intermetallic Compound	Oil	Reaction Temperature/°C	Time at Reaction Temperature/h
Bi_3Ni	Apricot kernel oil	280	48
Ni_3Sn_4	Safflower oil	270	6

Table 2-1: Synthetic conditions for binary intermetallics in edible oils

2.2.3 Characterization

Powder XRD data were collected at room temperature using a Bruker D8 Advance Diffractometer with a LynxEye 1-D-detector (Cu Kα radiation). Scanning electron microscopy (SEM), energy-dispersive X-ray spectroscopy (EDS), and elemental mapping data were collected using a JEOL JSM 5400 SEM operating at 20 kV.

2.3 Results and Discussion

The smoke points of apricot kernel and safflower oils are 257 ℃ and 249 ℃. For comparison, the melting points of Bi and Sn are 271 ℃ and 232℃. Accordingly, when Bi and Sn were added to these edible oils and heated to the appropriate temperature, the elemental metals become molten. Although the melting point of Bi is higher than the smoke point of the oil, it was observed that in an air-free environment the oils can be heated to ~30 ℃ above their smoke point without a noticeable increase in solvent degradation. As shown previously,[11] molten metal dispersions in organic solvents readily attack higher-melting metal powders,

forming intermetallic phases. This occurs *via* diffusion of the molten metal into the solid metal powders. Similar reactions occurred in the heated edible oils.

Figure 1 shows representative XRD data for Bi_3Ni and Ni_3Sn_4 intermetallics formed upon heating the lower melting metal (Bi, Sn) with the higher melting metal powders (Ni). Comparison of the simulated and experimental powder XRD patterns clearly confirms the formation of the intermetallic phases. Particularly, Bi_3Ni formed from the reaction of molten Bi with Ni in apricot kernel oil at 280 °C and Ni_3Sn_4 formed from the reaction of molten Sn with Ni in safflower oil at 270 °C. Here, the reaction times ranged from 6-48 h. These reaction times are equal to or longer than the times required using the glycol solvents.[11] The thermal stability of the oils is largely attributed to the high concentration of unsaturated fatty acids. The carboxylic acids are known to adhere more strongly than glycols to metals and oxide surfaces and have been shown to slow diffusion rates *via* surface passivation.[12] Since the reaction times were longer, the energy efficiency relative to the glycol-based solvent is lower; however, the use of non-toxic edible solvents helps to offset the concern. In both cases, the reactions occurred at significantly lower temperatures than traditional high-temperature metallurgical reactions, such as arc melting or dry powder processing.

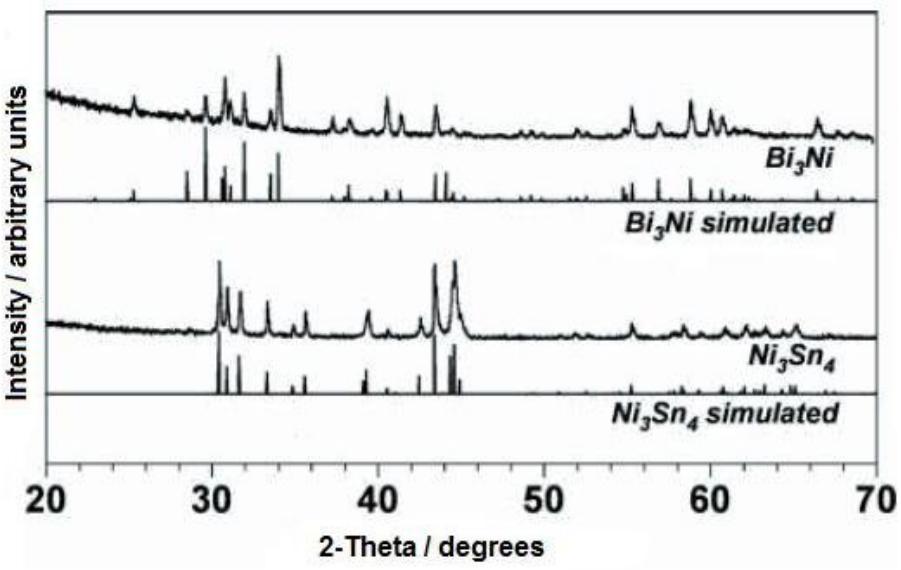

Figure 2-1: Powder XRD patterns of the binary intermetallic phases (*Figure was modified from the reference in chapter 2.6)*

The products formed from the reaction of bulk metal powders in heated edible oils are highly crystalline, as evident from the sharp XRD peaks in Figure 2-1, as well as the particle morphologies in Figure 2-2. In both intermetallic phases, preferred orientation is not observed by XRD, which is confirmed by the particle morphologies in Figure 2-2.

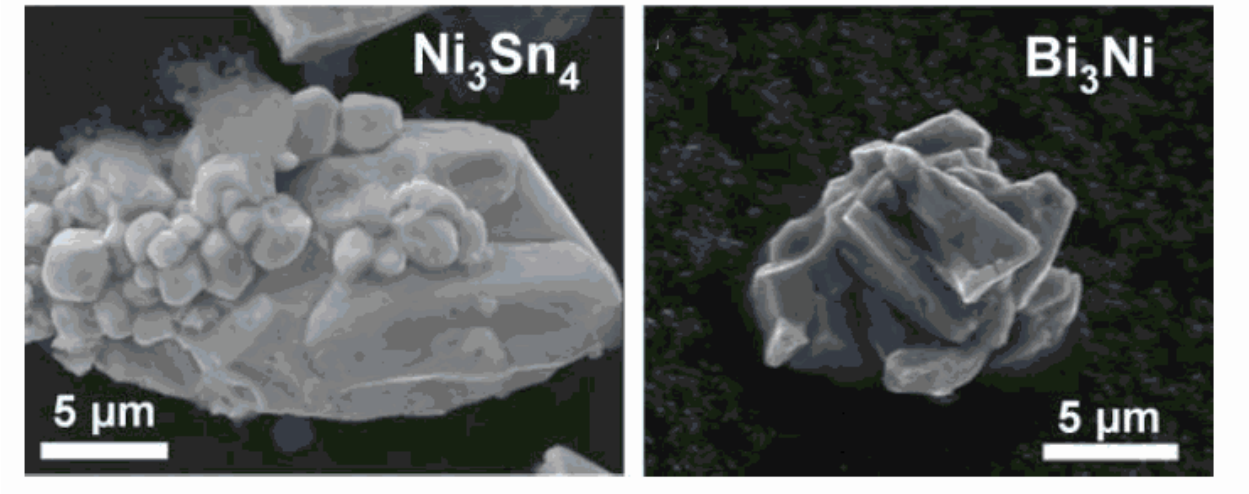

Figure 2-2: SEM images of Ni_3Sn_4 (left) and Bi_3Ni (right) (*Figure was modified from the reference in chapter 2.6*)

The chosen oils are largely composed of long chain fatty acids (*e.g.* oleic and linoleic acids), which gives rise to their high thermal stability.[15] Considering the similar compositions of these high-smoke point oils, the solvent choice can be determined based on other criteria, such as solvent availability and cost of production. Pertaining to the solvent, the Ni_3Sn_4 system in safflower oil was further studied to determine the recyclability of the solvent. Figure 2-3 shows powder XRD data from Ni_3Sn_4 synthesized in safflower oil at 250 °C for 48 h and the solvent subsequently reused. The Ni_3Sn_4 product was separated by centrifugation and fresh Ni and Sn powders were added to the previously-used oil. After heating again to 250 °C for an additional 48 h, phase-pure Ni_3Sn_4 was isolated. Three more cycles were completed, each successfully yielding Ni_3Sn_4. Although solvent degradation occurred, as indicated by a color change from yellow to brown, it is still re-usable for at least five cycles, or approximately 240 h. The fact that the intermetallic could be formed using the degraded oil implies that waste oil could be used as the reaction medium, providing an additional opportunity for recyclability. The re-usability of the edible oils after heating is significantly better than the glycols, which have been observed to degrade much faster at these reaction temperatures.

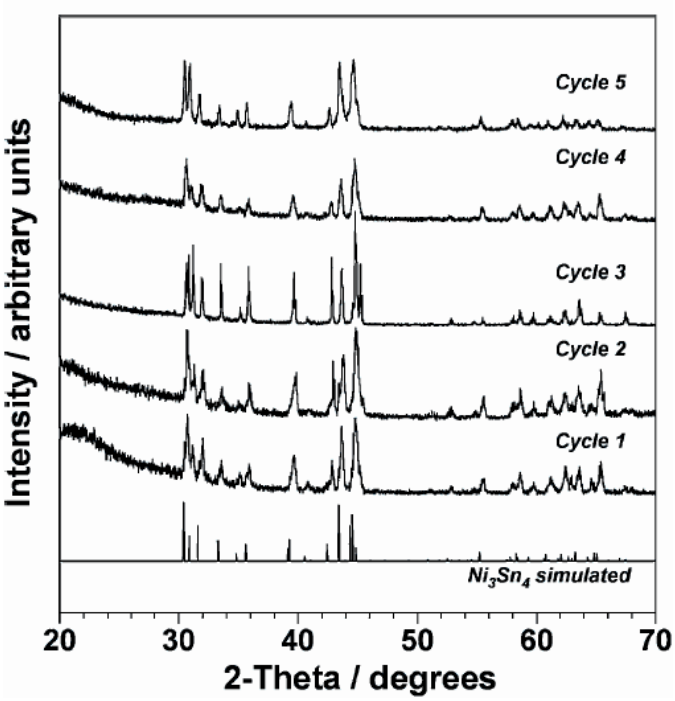

Figure 2-3: Powder XRD patterns for Ni_3Sn_4 recyclability study (formed at 250 °C) (*Figure was taken from the reference in chapter 2.6*)

2.4 Conclusion

A synthetic route for producing metallurgical solids in edible plant and seed oils was developed, providing a step towards green metallurgy. This low-temperature strategy yields bulk-scale intermetallics which are highly crystalline. The solvents used to synthesize them can be re-used several times, despite solvent degradation, as shown with the successful synthesis of the Ni_3Sn_4 phase repeatedly. The repeated synthesis of Ni_3Sn_4 confirms that the re-use of the solvent is feasible. In comparison to traditional metallurgical methods, such as arc melting and powder processing, reaction times are generally similar or shorter; however, the reaction temperatures are significantly lower. Compared to other solution-mediated reactions, the edible oils are a non-toxic alternative to most of the glycol-based systems.

2.5 References

1. Anastas, P. T.; Warner, J. C. *Green Chemistry; Theory and Practice.* Oxford University Press, Oxford, **1998,** *30*. Poliakoff, M.; License, P. *Nature.* **2007,** *450,* 810. Noyori, R. *Chem. Commum.* **2005,** 1807.

2. Mao, Y.; Park, T. J.; Zhang, F.; Zhou, H.; Wong, S. S. *Small.* **2007,** *3*, 1122. Murphy, C. J. *J. Mater. Chem.* **2008,** *18*, 2173.

3. Raveendran, P.; Fu, J.; Wallen, S. L. *Green Chem.* **2006,** *8*, 34. Koltypin, Y.; Perkas, N.; Gedanken, A. *J. Mater. Chem.* **2004,** *14*, 2975. Spear, S. K.; Griffin, S. T.; Granger, K. S.; Huddleston, J. G.; Rogers, R. D. *Green Chem.* **2007,** *9*, 1008.

4. Galkin, A. A.; Kostyuk, B. G.; Lunin, V. V.; Poliakoff, M. *Angew. Chem., Int. Ed.* **2000,** *39*, 2738. Cabanas, A.; Li, J.; Blood, P.; Chudoba, T.; Lojkowski, W.; Poliakoff, M.; Lester, E. *J. Supercrit. Fluids.* **2007,** *40*, 284. Aymonier, C.; Loppinet-Serani, A.; Reveron, H.; Garrabos, Y.; Cansell, F. *J. Supercrit. Fluids.* **2006,** *38*, 242. Fernandes, N. E.; Fisher, S. M.; Poshusta, J. C.; Valachos, D. G.; Tsapatsis, M.; Watkins, J. J. *Chem. Mater.* **2001,** *13*, 2023.

5. Mastrovito, C.; Lekse, J. W.; Aitken, J. A. *Solid State Chem.* **2007,** *180*, 3262. Lekse, J. W.; Pischera, A. M.; Aitken, J. A. *Mater. Res. Bull.* **2007,** *42*, 395.

6. Koch, C. C.; Whittenberger, J. D. *Intermetallic.* **1996,** *4*, 339. Meitl, M. A.; Dellinger, T. M.; Braun, P. V. *Adv. Funct. Mater.* **2003,** *13*, 795. Konrad, H.; Weissmuller, J.; Birringer, R.; Karmonik, C.; Gleiter, H. *Phys. Rev. B: Condens. Matter Mater. Phys.* **1998,** *58*, 2142.

7. Froes, F. H.; Senkov, O. N.; Baburaj, E. G. *Mater. Sci. Eng. A.* **2001,** *301*, 44. Ding, C.; Zhang, C.; Jianguo, C.; Zhenhua, C. *J. Alloys Compd.* **2008,** *461*, L23. Grigorieva, T. F.; Barinova, A. P.; Lyakhov, N. Z. *Russ. Chem. Rev.* **2001,** *70*, 45.

8. Kanatzidis, M. G.; Pottgen, R.; Jeitschko, W. *Angew. Chem., Int. Ed.* **2004,** *44*, 6996. Fisk, Z.; Remeika, J. P. *Handbook on the Physics and Chemistry of Rare Earths.* **1989,** 55.

9. Martin-Gonzalez, M.; Prieto, A. L.; Knox, M. S.; Gronsky, R.; Sands, T.; Stacy, A. M. *Chem. Mater.* **2003,** *15*, 1676. Onda, A.; Komatsu, T.; Yashima, T. *J. Catal.* **2001,** *201*, 13. Komatsu, T.; Inaba, K.; Uezono, T.; Onda, A.; Yashima, T. *Appl. Catal.* **2003,** *251*, 315. Mathur, S.; Veith, M.; Ruegamer, T.; Hemmer, E.; Shen, H. *Chem. Mater.* **2003,** *16*, 1304. Smalley, A. L. E.; Jespersen, M. L.; Johnson, D. C. *Inorg. Chem.* **2004,** *43*, 2486.

10. Roychowdhury, C.; Matsumoto, F.; Mutolo, P. F.; Abruna, H. D.; DiSalvo, F. J. *Chem. Mater.* **2005,** *17*, 5871. Karkamkar, A. J.; Kanatzidis, M. G. *J. Am. Chem. Soc.* **2006,** *128*, 6002. Leonard, B. M.; Bhuvanesh, N. S. P.; Schaak, R. E. *J. Am. Chem. Soc.* **2005,** *127*, 7326. Cable, R. E.; Schaak, R. E.; *J. Am. Chem. Soc.* **2007,** *19*, 4098. Cable, R. E.; Schaak, R. E. *J. Am. Chem. Soc.* **2006,** *128*, 9588. Cable, R. E.; Schaak, R. E. *Chem. Mater.* **2005,** *17*, 6835. Schaak, R. E.; Sra, A. K.; Leonard, B. M.; Cable, R. E.; Bauer, J.

C.; Han, Y.-F.; Means, J.; Teizer, W.; Vasquez, Y.; Funck, E. S. *J. Am. Chem. Soc.* **2005,** *127,* 3506. Chou, N. H.; Schaak, R. E. *Chem. Mater.* **2008,** *20,* 2081. Chou, N. H.; Schaak, R. E. *J. Am. Chem. Soc.* **2007,** *129,* 7339. Alden, L. F.; Roychowdhury, C.; Matsumoto, F.; Han, D. K.; Zeldovich, V. B.; Abruna, H. D.; Disalvo, F. J. *Langmuir.* **2006,** *22,* 10465. Roychowdhury, C.; Matsumoto, F.; Zeldovich, V. B.; Warren, S. C.; Mutolo, P. F.; Ballesteros, M. J.; Weisner, U.; Abruna, H. D.; Disalvo, F. J. *Chem. Mater.* **2006,** *18,* 3365.

11. Henderson, N. L.; Schaak, R. E. *Chem. Mater.* **2008,** *20,* 3212.

12. Lu, X.; Tuan, H. –Y.; Chen, J.; Li, Z. –Y.; Korgel, B. A.; Xia, Y. *J. Am. Chem. Soc.* **2007,** *129,* 1733. Willis, A. L.; Turro, N. L.; O-Brien, S. *Chem. Mater.* **2005,** *17,* 5970.

13. Lang, A.; Jeitschko, A. *Z. Metallkd.* **1996,** *87,* 759.

14. Larsson, A. –K.; Stenberg, L.; Lidin, S. *Acta Cryst.* **1994,** *B50,* 636.

15. Fuller, G.; Kohler, G. O.; Applewhite, T. H. *J. Am. Oil Chem. Soc.* **1966,** *43,* 477. Frankel, N. *J. Am. Oil Chem. Soc.* **1993,** *70,* 767.

16. Ingold, K. U. in *Lipids and Their Oxidation,* ed. Schultz, H. W.; Day, E. A.; Sinnhaber, R. O. AVIPublishing Co., Westport, CT, USA, **1962,** 93-121. Donovan, D. H.; Menzel, D. B. *Cell. Mol. Life Sci.* **1978,** *34,* 775. Maheswari, S. U.; Ramadoss, C. S.; Krishnaswamy, P. R. *Mol. Cell Biol.* **1997,** *177,* 47.

17. Halliwell, B.; Murcia, M. A.; Chirico, S.; Aruoma, O. I. *Crit. Rev. Food Sci. Nutr.* **1995,** *35,* 7. Min, D. B.; Wen, J. *J. Food Sci.* **1983,** *48,* 1429.

2.6 Publication

Henderson, N. L.; Straesser, M. D.; Sabato, P. E.; Schaak, R. E. Toward green metallurgy: low temperature solution synthesis of bulk-scale intermetallic compounds in edible plant and seed oils. *Green Chem.* **2009,** 11, 974-978.

2.7 Acknowledgement of Collaborative Work

The aforementioned work was completed in collaboration with Henderson, Sabato, and Schaak. Additional published work, not listed here, can be found in the publication.

Chapter 3

Sodium Nitrite Oxidation

3.1 Introduction

Metal oxides are traditionally synthesized by reacting the zero-valent metal(s) with oxygen at extremely high-temperature reactions. One example of a high-temperature reaction is furnace annealing.[1] However, this technique generates a product with no morphology control and requires harsh, high-temperature conditions. Another synthetic technique used to synthesize metal oxides is the use of a metastable solid solution. For example, tin oxide nanoparticles have been synthesized using a metastable solid solution.[2] The metastable solid solution was synthesized by doping the tin oxide crystals with rare earth elements, La_2O_3, Nb_2O_5, and CeO_2. In this study, the dopants were incorporated into the crystal lattice of SnO_2 and the dopant's presence depressed the growth rate of the crystals. By controlling the concentration of the dopant, the SnO_2 nanoparticle sizes were controlled. At higher temperatures, the doped SnO_2 nanoparticles phase segregated. Although this process produced size-controlled SnO_2 nanoparticles, the reaction is both time and energy intensive, requiring long heating and high-temperatures. An area which has received less attention is solution-mediated nanoparticle oxidation.[3,4] Solution-mediated oxidations primarily have been focused on using oxygen as the oxidizing agent.[4] For example, air is commonly used to oxidize iron nanoparticles into iron oxide nanoparticles. The reaction is achieved by bubbling air into the reaction media at elevated temperatures for time periods of 16-24 hrs. Despite the known utility of common organic and inorganic oxidizing agents, there has been limited research conducted on the use of oxidizing agents applied to solution-mediated nanoparticle oxidation. There are several advantages of using a chemical oxidizing agent as opposed to using air or the traditional methods. One such

advantage is the reaction time. Using a chemical oxidizer usually allows for much faster reaction times by comparison to overnight heating in air. Chemical oxidizing agents can also have much stronger oxidation potentials. For example, chromic acid and potassium permanganate have standard reduction potentials of 1.33 eV[5] and 1.51 eV;[5] by comparison, oxygen has a reduction potential of 1.23 eV.[5] These values were obtained using the standard hydrogen electrode. Another advantage to using chemical oxidizing agents is retention of the particle's morphology. Traditional high-temperature oxidizing methods usually destroy the particle's morphology.

Sodium nitrite ($NaNO_2$) has long been known to oxidize amines into nitrosamine compounds. In an acidic media, the nitrosamines are converted to diazonium ions.[6] The synthetic utility of the diazonium ion is to serve as a more facil leaving group in an S_N2 substitution. In organic synthesis, $NaNO_2$ also is used to destroy excess azides.[7] By comparison, potassium permanganate and chromic acid are commonly used to oxidize alcohols to ketones and further to carboxylic acids.[8] Potassium permanganate also has been known to cleave alkenes into ketones and aldehydes.[8] $NaNO_2$ is by no means as strong of an oxidizer as potassium permanganate and chromic acid; the presence of alcohols and alkenes from either the solvent or the surface stabilizer renders the use of strong oxidizing agents futile. Despite the known oxidizing strength of $NaNO_2$, there are no reports of it being applied to oxidize metal nanoparticles.

There are various advantages in using $NaNO_2$ as a chemical oxidizing agent. $NaNO_2$ is highly soluble in polar media (solubility in water = 82 g mL^{-1}).[9] $NaNO_2$ relatively high solubility makes the dissolution of $NaNO_2$ into polar orgaic media, such as polyols and dimethyl sulfoxide (DMSO), feasible. Also, $NaNO_2$ has relatively high thermal stability by comparison to other oxidizing agents. For example, $NaNO_2$, $NaNO_3$ CrO_3, $KMnO_4$, and OsO_4 have

decomposition temperatures of 271, 306, 196, 240, and 130 °C.[9-13] The decomposition temperatures imply that $NaNO_2$ can be heated to higher temperatures without thermal decomposition. $NaNO_2$ toxicity is also significantly lower than other chemical oxidizers in its class. In fact, $NaNO_2$ commonly serves as a vasodilator in medical applications as well as a curing and preserving agent in the food industry.[14]

The chemical oxidation of metal nanoparticles was accomplished by dissolving $NaNO_2$ in a high boiling polyol or non-reducing DMSO solvent. The $NaNO_2$ solution was subsequently added to a disperision of either Te, Bi, Sn, In, or Pb metal nanoparticles. There are some limitations to this oxidizing method. One limitation associated with using DMSO is the reaction temperature, limited by the solvent's boiling point (189 °C). On the other hand, using a high boiling solvent, such as tetraethlyene glycol (TEG), allows the reaction to be heated to 300 °C; however, the reducing strength of the glycol becomes significantly stronger as the temperature is raised. Thus, the reducing potential of the solvent counteracts the oxidizing potential of the $NaNO_2$.

3.2 Experimental

3.2.1 Materials

All chemicals were purchased and used without further purification: $SnCl_2$ (Alfa Aesar, 99%), polyvinylpyrrolidone (PVP) (average m.w. = 630K and 40K, Alfa Aesar), $NaBH_4$ (Alfa Aesar, 98%), $Pb(C_2H_3O_2)_4$ (Sigma Aldrich, 99.99 %), $Pb(NO_3)_2$ (Sigma Aldrich, 99.999%), $Bi(NO_3)_3 \cdot 5H_2O$ (Alfa Aesar, 98%), $InCl_3$ (Alfa Aesar, 99.999%), $H_2TeO_4 \cdot 2H_2O$ (Alfa Aesar, 99%), $NaNO_2$ (Sigma Aldrich, 99%), tetraethylene glycol (TEG, Alfa Aesar, 98%), diethylene glycol (DEG, Alfa Aesar, 99%), ethylene glycol (EG, Alfa Aesar, 99%), dimethyl sulfoxide

(DMSO, Alfa Aesar, 99.8%), 2 mol/L $NaBH_4$ solution in Diglyme (Sigma Aldrich, 99%). All reactions were completed using air free techniques in 3 neck flasks. All reactions were cooled to room temperature before being worked-up.

3.2.2 Synthesis

3.2.2.1 Sn Nanoparticles

Sn nanoparticles were synthesized by dissolving the PVP (630K, 0.250 g) and $SnCl_2$ (0.2 mmol) in 5 mL TEG each by sonication. The PVP and $SnCl_2$ were added to 10 mL TEG and purged with Ar under vigorous stirring (800-1100 rpm). The temperature of the reaction was raised (~5 °C/min) to 90 °C and 5 drops of $NaBH_4$ (2.0 mmol dissolved in 5 mL TEG) was added to the reaction at the rate of 1 drop/sec. The reaction mixture turned dark red and the temperature was raised to 120 °C. 10 drops of the $NaBH_4$ solution was added again at 120 °C and at 150 °C, both at a rate of 1 drop/sec. After the second addition the reaction mixture turned black. The temperature was raised to 180 °C and the rest of the $NaBH_4$ solution was added at a rate of 2 drops/sec. The reaction temperature was raised to 220 °C, aged for 30 min, and then stopped. After cooling to room temperature, the reaction mixture was diluted 3:1 (acetone: TEG) and centrifuged at 8000 rpm for 7 min. The collected particles were then suspended in 2:1 (ethanol: hexanes) and centrifuged at 8000 rpm for 5 min. The ethanol: hexanes washes were completed twice and the particles were finally stored in ethanol.

3.2.2.2 SnO_2 Nanoparticles

Half of the pre-synthesized Sn particles (~0.1 mmol) were suspended *via* sonication in 1.5 mL EG. The particles were then added to 10 mL of EG. $NaNO_2$ (0.25 g), dissolved *via*

sonication in 8.5 mL EG, subsequently was added to the reaction. The reaction mixture was purged with Ar and vigorously stirred (800-1100 rpm) for the entire reaction. The temperature of the reaction was rapidly (~5 °C/min) raised to 40 °C for 1 hr and then raised to 140 °C for 14 hrs before being stopped. The reaction was diluted 3:1 with ethanol and centrifuged 10000 rpm for 3 min. The particles were re-suspended in ethanol and centrifuged at 10000 rpm for 5 min. These washes were completed 3x and the particles were stored in ethanol.

3.2.2.3 Bi Nanoparticles

The following procedure was modified from a published procedure.[15] PVP (40K, 0.5012 g) and $Bi(NO_3)_3 \cdot 5H_2O$ (0.0475 g) were dissolved *via* sonication in 25 mL TEG. The reaction mixture was then purged with Ar and heated rapidly (~5 °C/min) to 190 °C under vigorous (800-1100 rpm) stirring. At 190 °C, the $NaBH_4$ (0.0286 g, dissolved *via* sonication in 2 mL TEG) was injected at 1 drop/sec. Upon the injection, the reaction mixture turned black. The temperature of the reaction was raised to 230 °C for 1 hr and then stopped. The reaction mixture was diluted 3:1 (acetone: TEG) and centrifuged at 8000 rpm for 5 min. The particles were re-suspended in 1:1 (ethanol: hexanes) and centrifuged at 8000 rpm for 4 min. The 1:1 (ethanol: hexanes) washes were completed 3x and the particles were then stored in ethanol.

3.2.2.4 Bi_2O_3 Nanoparticles

Half of the pre-synthesized Bi nanoparticles (~0.005 mmol) were suspended *via* sonication in 1.5 mL DMSO and $NaNO_2$ (0.250 g) was dissolved *via* sonication in 3.5 mL DMSO. The nanoparticles and $NaNO_2$ were added to 10 mL DMSO, purged with Ar, and the reaction was rapidly (~5 °C/min) heated to 160 °C under vigorous stirring (800-1100 rpm). The reaction mixture was kept at 160 °C for 14 hrs and then stopped. The reaction mixture was

diluted 3:1 (acetone: TEG) and centrifuged at 12000 rpm for 5 min. The nanoparticles were re-suspended in ethanol and centrifuged at 13500 rpm for 5 min. The ethanol washes were completed 3x and the particles were stored in ethanol.

3.2.2.5 Pb Nanoparticles

The following procedure was modified from a published preparation.[16] PVP (630K, 0.250 g) was dissolved *via* heat and stirring into 5 mL DEG. $Pb(C_2H_3O_2)_4$ (0.1 mmol) and $Pb(NO_3)_2$ (0.1 mmol) were dissolved in 5 mL DEG *via* sonication. The PVP was added to 10 mL DEG and purged with Ar. The reaction mixture was rapidly (~5 °C/min) heated to 230 °C under constant vigorous stirring (800-1100 rpm) and then the Pb precursors were injected using a syringe pump at a rate of 0.25 mL/min. After the injection, the reaction mixture was aged for 1 hr at 230 °C and then stopped. The reaction mixture by this point had turned black. The reaction mixture was diluted 3:1 (ethanol: DEG) and centrifuged at 13500 rpm for 5 min. The particles were re-suspended in ethanol and centrifuged at 12000 rpm for 5 min. The ethanol washes were completed 3x and the particles were stored in ethanol.

3.2.2.6 Pb_xO_y Nanoparticles

Half of the pre-synthesized Pb nanoparticles (~0.1 mmol) were suspended in 1.5 mL of TEG *via* sonication. The Pb nanoparticles were added to 10 mL TEG, purged with Ar, and the reaction was rapidly heated to 140 °C under constant vigorous stirring (800-1100 rpm). $NaNO_2$ (0.250 g), dissolved in 5 mL TEG *via* sonication, was injected at 140 °C slowly using a syringe pump (0.083 mL/min). During the injection, the reaction mixture was increased to 220 °C and the reaction was aged 20 min at 220 °C before being stopped. The reaction mixture was diluted 3:1 (ethanol: TEG) and centrifuged at 12000 rpm for 5 min. The collected particles were re-

suspended in ethanol and centrifuged at 8000 rpm for 4 min. The ethanol washes were completed 3x and the particles stored in ethanol.

3.2.2.7 Te Nanoparticles

PVP (40K, 0.223 g) was dissolved in 15 mL EG *via* sonication and $H_2TeO_4 \cdot 2H_2O$ (0.0476 g) was dissolved *via* sonication in 5 mL EG. The PVP and Te precursor were combined, purged with Ar, and rapidly heated to 180 °C under continuous vigorous (800-1100 rpm) stirring. At 185 °C, the reaction mixture turned black and $NaBH_4$ (2 mmol) dissolved in 1 mL diglyme was injected to ensure complete reduction. The temperature of the reaction mixture was raised to reflux and aged 40 min before being stopped. The nanoparticles were diluted 3:1 (acetone: EG) and centrifuged at 8000 rpm for 5 min. The collected particles were re-suspended in 1:1 (ethanol: hexanes) and centrifuged at 8000 rpm for 4 min. The ethanol: hexanes washes were completed 3x and the nanoparticles were stored in ethanol.

3.2.2.8 TeO_2 Nanoparticles

Half of the pre-synthesized Te nanoparticles (~0.05 mmol) were suspended *via* sonication in 1.5 mL TEG and added to 10 mL of TEG. $NaNO_2$ (0.252 g), dissolved in 5 mL TEG *via* sonication, was subsequently added to the reaction. The reaction mixture was purged with Ar and rapidly (~5 °C/min) heated to 220 °C for 14 hrs under vigorous (800-1100 rpm) stirring. The reaction mixture was stopped, diluted 3:1 (acetone: TEG) and centrifuged at 12000 rpm for 5 min. The collected nanoparticles were re-suspended in ethanol and centrifuged at 13500 rpm for 5 min. The ethanol washes were completed 3x and the particles were stored in ethanol.

3.2.2.9 In Nanoparticles

PVP (630K, 0.250 g), $InCl_3$ (0.045 g) and $NaBH_4$ (0.113 g) were dissolved *via* sonication in 5 mL TEG each. The PVP and the $InCl_3$ were combined with 5 mL TEG, purged with Ar and rapidly (~5 °C/min) heated to 90 °C under continuous vigorous stirring (800-1100 rpm). At 90 °C, the $NaBH_4$ was injected slowly (1 drop/sec) and the reaction mixture turned grey, indicating reduction. The reaction mixture was rapidly raised to 150 °C and aged 30 min before being stopped. The reaction mixture was then diluted 3:1 (acetone: TEG) and then centrifuged at 8000 rpm for 5 min. The collected nanoparticles were then re-suspended in 1:1 (ethanol: hexanes) and centrifuged at 8000 rpm for 4 min. The ethanol: hexanes washes were completed 3x and the nanoparticles stored in ethanol.

3.2.2.10 In_2O_3 Nanoparticles

Half of the pre-synthesized In nanoparticles (~0.1 mmol) were suspended *via* sonication in 1.5 mL DMSO. The suspended nanoparticles were added to 10 mL DMSO and purged with Ar. $NaNO_2$ (0.250 g), dissolved in 3.5 mL DMSO *via* sonication, was then subsequently added to the reaction mixture, which was under continuous vigorous stirring (800-1100 rpm). Upon the addition, the reaction mixture turned instantly from grey to black. The reaction mixture was rapidly (~5 °C/min) heated to 100 °C for 2 hrs and then raised to 150 °C for 2 hrs before being stopped. The reaction mixture was diluted 3:1 (acetone: DMSO) and centrifuged at 8000 rpm for 5 min. The collected nanoparticles were then re-suspended in 1:1 (ethanol: hexanes) and centrifuged at 8000 rpm for 4 min. The ethanol: hexanes washes were completed 3x and then 3 more ethanol alone washes were completed (centrifuging at 12000 rpm for 5 min). The particles were then stored in ethanol after a total of 6 washes.

3.2.3 Characterization

Powder XRD data were collected at room temperature using a Bruker D8 Advance Diffractometer with a LynxEye 1-D-detector (Cu Kα radiation). Transmission electron microscopy (TEM) images and selected area electron diffraction (SAED) patterns were obtained from a JEOL 1200 EX II operating at 80 kV.

3.3 Results and Discussion

As indicated by the XRD patterns, the transformation of Sn, Pb, and In, to presumably their respective oxides, was successfully completed using $NaNO_2$ as an oxidizing agent. Bi and Te showed some degree of oxidation; however, neither were completely oxidized. The standard reduction potentials, using the standard hydrogen electrode as the reference electrode, of Sn^{2+}, Bi^{3+}, Pb^{2+}, Te^{6+}, and In^{3+} to their most oxidized forms are -0.14, +0.308, -0.13, +1.02, and -0.34 eV, respectively.[17] Considering that partial oxidation was seen in the Te nanoparticle system, it would indicate that the oxidation strength of the $NaNO_2$ is at least 1.02 eV, referenced from the standard reduction potential of Te. In the case of TEG, the reduction potential of the solvent becomes significant as the temperature is increased. It is well known that TEG can thermally reduce Pb^{2+} and Pb^{4+} salts at temperatures above 200 °C. The inherent reduction potential of the solvent would therefore counteract the oxidation potential of the $NaNO_2$ and thus weaken its strength. Although DMSO is a non-reducing solvent, unlike the glycols, it cannot be heated as high as the glycols, and so thermally increasing the oxidation potential of the $NaNO_2$ becomes difficult.

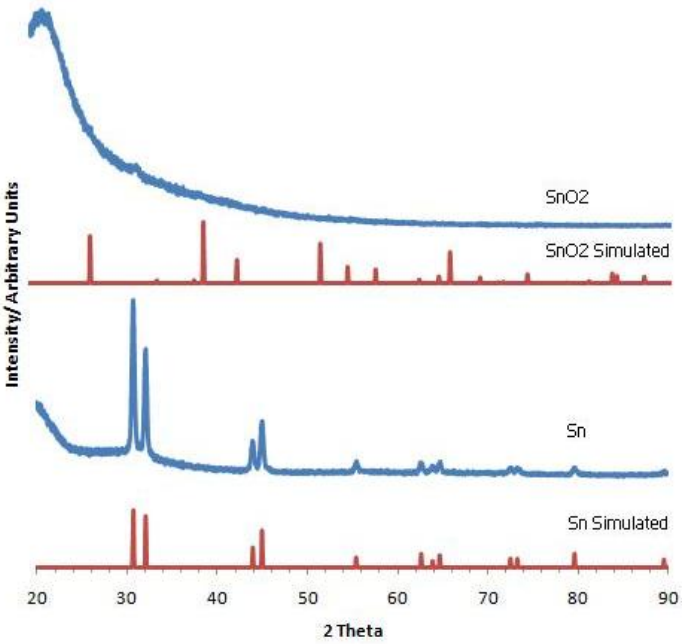

Figure 3-1: Powder XRD patterns of Sn and SnO_2

The powder XRD patterns of the Sn and the SnO_2 nanoparticles clearly indicates that the crystallinity of the Sn nanoparticles was destroyed as a result of the oxidation. Although SnO_2 is not indicated by the powder XRD pattern, it is assumed to be formed over SnO because the nanoparticles turned from black to white as a result of the oxidation reaction. This indicates that SnO_2 was likely formed because it is white while SnO is black.

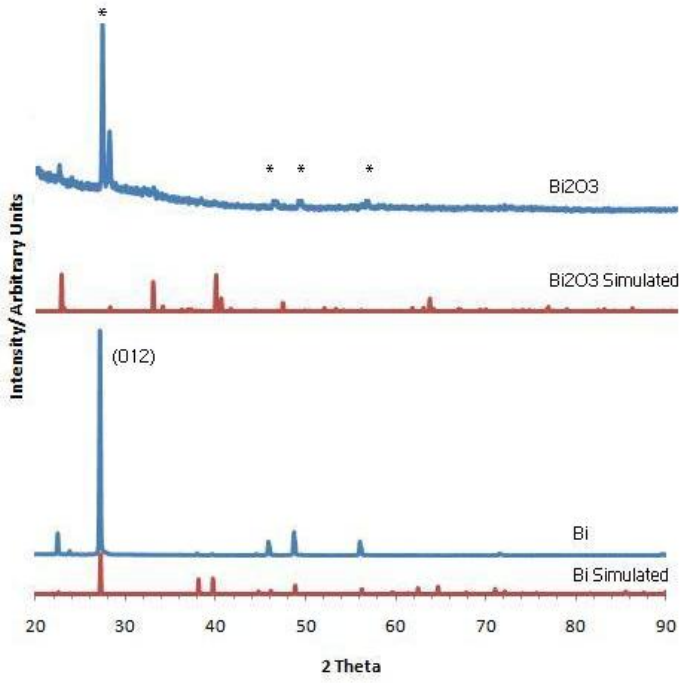

Figure 3-2: Powder XRD patterns of Bi and Bi_2O_3. (* Indicates non-oxidized Bi Peaks)

As seen in the powder XRD patterns of Bi and Bi_2O_3, perferred orientation is observed. The preferred orientation is most notable in the Bi pattern where the (012) plane is showing the strongest intensity. In the Bi_2O_3 XRD pattern, preferred orientation is also observed. The largest oxide peak is seen next to the (012) Bi peak. Using this oxide peak, it can be estimated that the reaction proceeded to ~20% oxide.

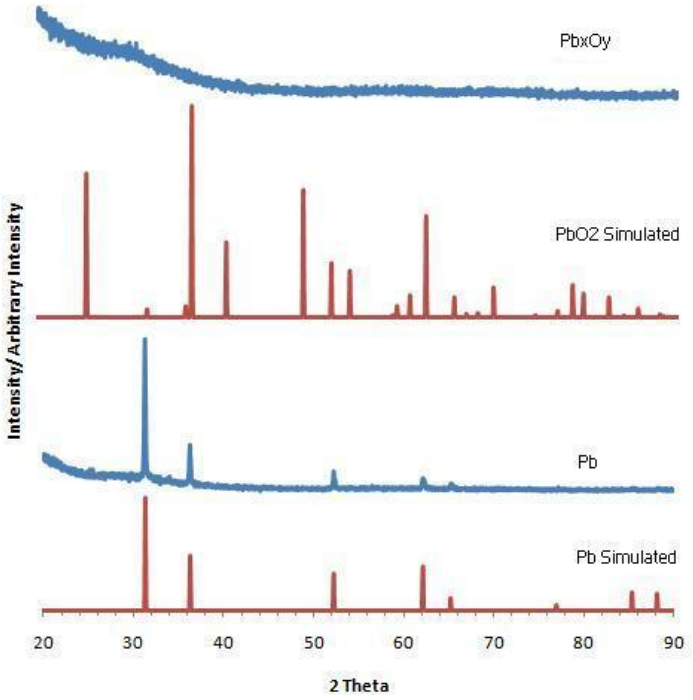

Figure 3-3: Powder XRD patterns of Pb and Pb_xO_y

As seen in the powder XRD patterns for Pb and Pb_xO_y, all crystallinity was destroyed as a result of the oxidation reaction. Although the PbO_2 phase was used for the simulated pattern, it is possible that mixed oxide phases were present. Other oxide phases that could be present are PbO and Pb_3O_4; however, PbO_2 and Pb_3O_4 would likely be the largest contributors since they are the most oxidized states of lead.

Upon further heating in TEG, the Pb_xO_y nanoparticles were reduced back to their zero-valent crystalline form. This was confirmed by XRD, although not shown here. This is supporting evidence that the reducing potential of the glycol solvent can counteract the oxidizing potential of the $NaNO_2$.

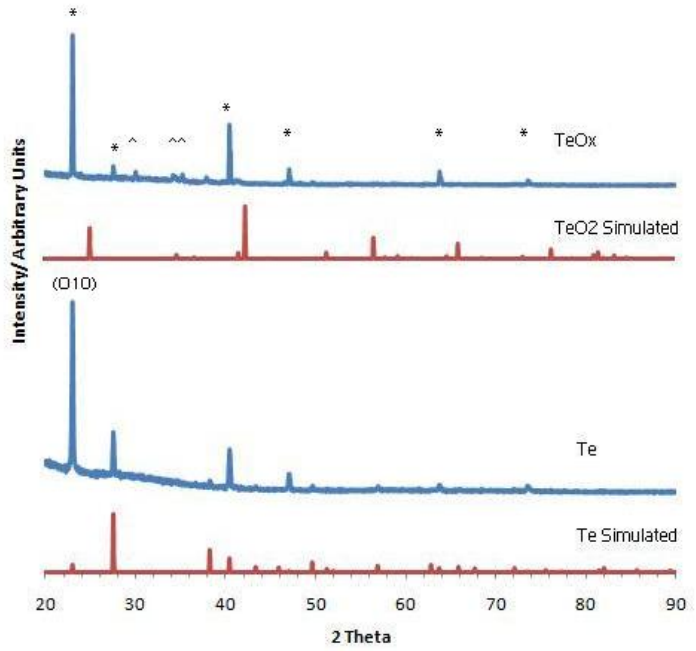

Figure 3-4: Powder XRD patterns of Te and TeO_2. (* Indicates non-oxidized Te peaks. ^ Indicates possible TeO_2 peaks)

The powder XRD pattern of Te and TeO_2 shows preferred orientation in the Te pattern with the (010) plane. The preferred orientation accounts for the height differences observed in the Te peaks. The TeO_2 pattern shows minimal (~5%) oxidation of the Te nanoparticles. TeO_2 is possibly observed in the XRD pattern. Several peaks between 30°-40° indicate the presence of a species other than Te. Although not all the peaks directly match to TeO_2, it is possible that TeO_2 is present due to the loss of intensity observed in the Te peaks and the presence of new peaks between 30°-40°. The differences in the peak intensities can be attributed to the initial preferred orientation of the Te particles. The initial preferred orientation would lead to non-equal exposure of the crystal faces to the NO_2^- oxidizer and thus the oxide faces may not have grown equally.

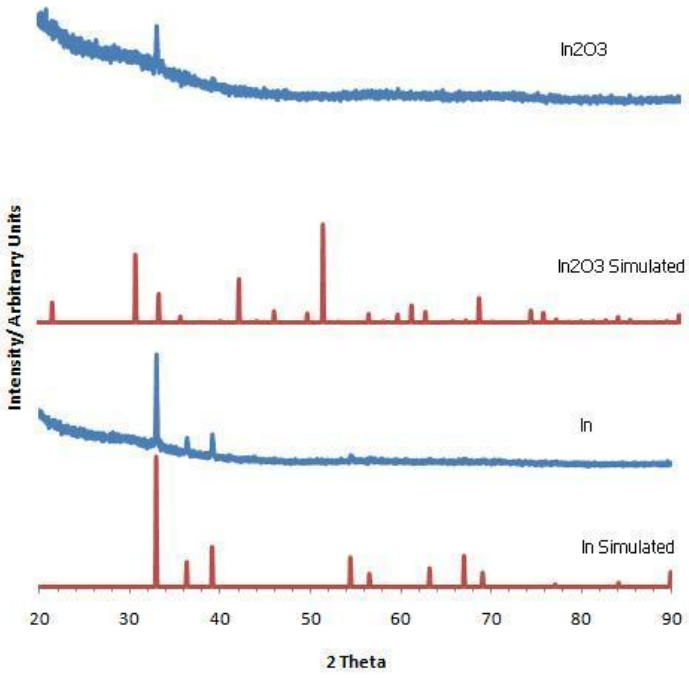

Figure 3-5: Powder XRD patterns of In and In_2O_3

The powder XRD patterns of In and In_2O_3 indicate that most of the crystallinity of the In nanoparticles was destroyed as a result of the oxidation reaction. However, a little In peak can be seen in the In_2O_3 pattern. Although the XRD cannot confirm the presence of In_2O_3, it is assumed that it formed because the metallic In nanoparticles turned from a shiny metallic color to white as a result of the oxidation reaction.

A trend observed with the NO_2^- oxidation is that the crystallinity of the In, Sn, and Pb nanoparticles was destroyed as a result of the oxidation reaction. A possible reason why the crystallinity of the nanoparticles was destroyed is that as oxygen atoms diffused into the crystal lattices of the nanoparticles, they could have disrupted the lattices. This disruption could have lead to the destruction of the crystallinity. Since the reactions were conducted at relatively low-

temperatures it is likely that not enough thermal energy was given to recrystallize the formed oxide particles.

Partial oxidation was seen in the Bi and Te nanoparticle systems. The likely reason for the partial oxidation of the Bi and Te nanoparticles is that Bi and Te have standard reduction potential of 0.308 and 1.02 eV. This shows that oxidizing Bi and Te is not thermodynamically favored. The thermodynamic disfavor of the reaction would slow the rate oxidation and thus explain the partial oxidations. Another possible explanation for the partial oxidation of the Bi and Te nanoparticles is that the formed oxides could have formed an oxide coating around the particle and the oxide coating could have acted as a diffusion barrier for more oxygen. A classical example of a protecting oxide is Al_xO_y, which protects the Al beneath its coating from oxidizing. A counter example is Fe_2O_3, which does not protect Fe below the oxide surface from oxidizing. Surface oxide barriers, where the diffusion rate of oxygen through the oxide is much slower than that of the metal, may have occurred in the Bi_2O_3 and TeO_x nanoparticle systems.

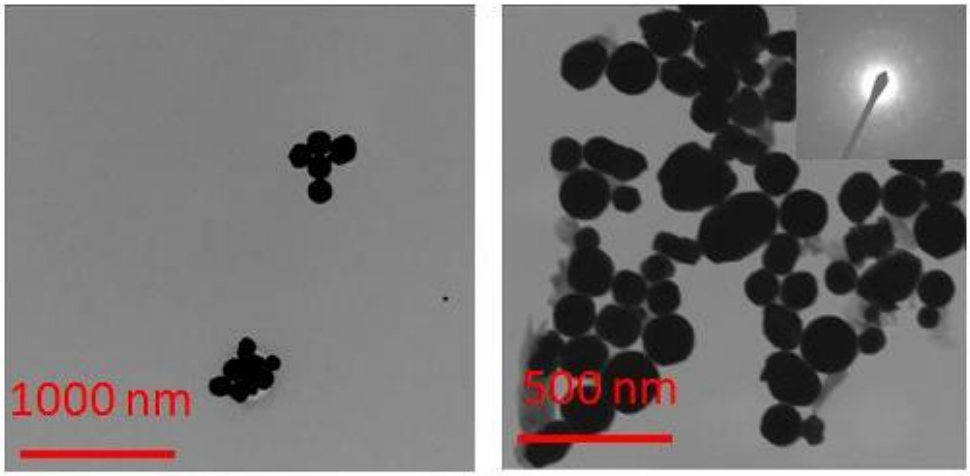

Figure 3-6: TEM images of Bi (left) and Bi_2O_3 (right). SAED pattern of Bi_2O_3 showing polycrystalline rings and spots, consistent with mixed phases

The TEM images of Bi and Bi_2O_3 nanoparticles confirms that the morphology of the Bi nanoparticles was preserved throughout the oxidation reaction. The morphology of the Bi nanoparticles also is consistent with the preferred orientation in the powder XRD pattern. The SAED pattern of the Bi_2O_3 confirms that the sample is polycrystalline, which is consistent with the mixed phases. Although a polycrystalline SAED is consistent with mixed-phases, it does not necessarily confirm the presence of Bi and Bi_2O_3. The mixed phases which are present are the crystalline Bi and crystalline Bi_2O_3. The likely morphology for the nanoparticles is a Bi_2O_3 coating with a Bi core.

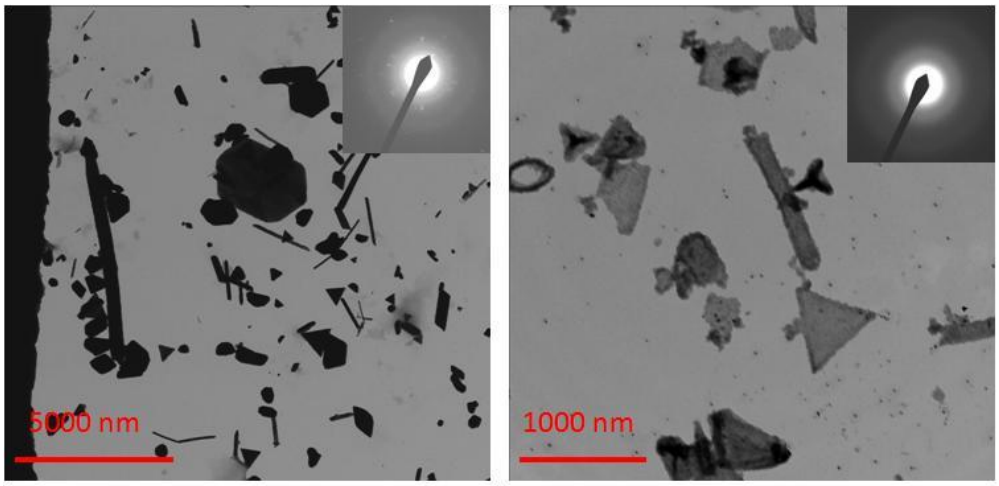

Figure 3-7: TEM images of Pb (left) and Pb_xO_y (right). SAED pattern of Pb (left) showing spots consistent with crystalline nanoparticles. SAED pattern of Pb_xO_y (right) showing only amorphous broad rings, which is consistent with the powder XRD pattern

The TEM images of the Pb and Pb_xO_y nanoparticles confirms that the Pb nanoparticles morphology was maintained throughout the oxidation reaction. The SAED patterns of the Pb and Pb_xO_y confirms that the crystallinity of the Pb nanoparticles was destroyed as a result of the oxidation reaction. Also, the Pb nanoparticles fairly blocked out all electron beam penetration

while the Pb_xO_y nanopartciles allowed a substantial amount of beam penetration through the particles. The electron beam penetration is consistent with the oxidation of the nanoparticles.

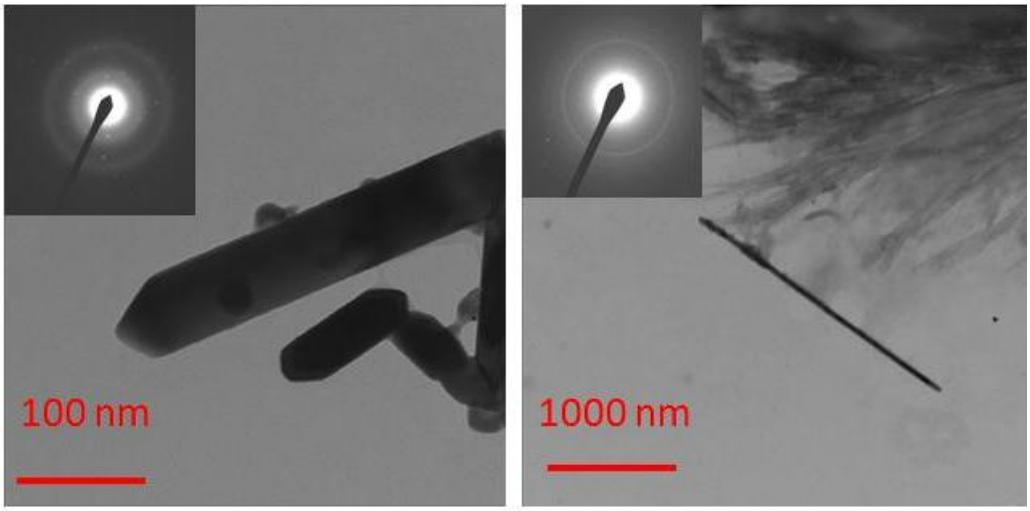

Figure 3-8: TEM images of Te (left) and TeO_2 (right). SAED pattern of Te nanoparticles (left) showing spots and polycrystalline rings. SAED pattern of TeO_2 nanoparticles (right) showing polycrystalline rings, consistent with mixed phases

The TEM images of the Te and TeO_2 nanoparticles shows that the Te nanoparticle morphology was preserved in the oxidation reaction. The morphology of the Te nanoparticles is also consistent with the preferred orientation seen in the powder XRD pattern. The SAED pattern of the TeO_2 nanoparticles confirms the polycrystalline nature of the particles. Also, the TeO_2 nanowire shows jagged growth of the side of the particle. This jagged growth is consistent with oxide growth. As seen in the TEM image of the Te nanoparticles, none of the Te nanoparticles shows jagged growths.

The morphology of the Pb, Te, and Bi nanoparticles was somewhat preserved throughout the oxidation reaction, as confirmed by the TEM images. Also, the SAED pattern of the Pb_xO_y nanoparticles confirmed that the sample was amorphous and that all crystallinity, as seen in the

SAED pattern of the Pb nanoparticles, was destroyed. The SAED patterns of TeO_2 and Bi_2O_3 nanoparticles confirmed that samples were polycrystalline, which is consistent with a mix of oxide phases and the metallic phases.

3.4 Conclusions

The oxidation of Sn, Bi, Pb, Te, and In were studied using $NaNO_2$ as the oxidizing agent. Although the crystallinity of Sn, In, and Pb was completely destroyed, it is likely that the particles oxidized. Qualitative evidence leading to the particles oxidation were the color changes observed in the In and Sn systems. The black-to-white color change observed in the Sn to SnO_2 reaction is consistent with the oxidation of the Sn nanoparticles. The disappearance of the shiny metallic color in the In system is also consistent with the oxidation of the In nanopartices. Bi and Te were only partially oxidized but that is likely due to the size of the nanoparticles and the oxide coating acting as a diffusion barrier. The nanoparticle morphology was somewhat preserved during the oxidation of the Te, Pb, and Bi nanoparticle systems. All of this evidence points to the potential applications of $NaNO_2$ as a chemical oxidizing agent for low reduction potential metal nanoparticle systems.

In future work, to determine the chemical state of the surfaces of the SnO_2, Bi_2O_3, Pb_xO_y, TeO_2, and In_2O_3 nanoparticles, XPS (X-ray photoelectron spectroscopy) measurements could be conducted. This would determine if the surfaces of the SnO_2, Pb_xO_y, and In_2O_3 nanoparticles were actually oxidized. To further oxidize the Bi and Te systems, perhaps a stronger oxidizing agent, such as potassium permanganate, could fully oxidize the nanoparticles. A solvent study using the Bi nanoparticle system could also be conducted to determine if the glycols reducing potential counteracts the oxidizing potential of the $NaNO_2$.

3.5 References

1. Lee, J.; Sim, S.; Kim, K.; Cho, K.; Kim, S. *Mater. Sci. Engr. B.* **2005,** *122,* 85-89.

2. Leite, E.; Maciel, A.; Weber, I.; Lisboa-Filho, P.; Longo, E.; Paiva-Santos, C.; Andrade, A.; Pakoscimas, A.; Maniette, Y.; Schreiner, W. *Adv. Mater.* **2002,** *14,* 905-908.

3. Wang, W.; Yao, J. *J. Phys. Chem. C.* **2009,** *113,* 3070-3075.

4. Sarka, A.; Chadha, R.; Mukherjee, T.; Kapoor, S. *Chem. Phys. Letters* **2009,** *473,* 111-115.

5. Brown, T.; LeMay, H.; Bursten, B. *Chemistry the Central Science,* 10th ed.; Pearson: Upper Saddle River; 2006; p 1128.

6. Cohen, T.; Dietz, A.; Miser, J. *J. Org. Chem.* **1977,** *42,* 2053-2058.

7. The National Academies Press, Prudent Practices in the Laboratory: Handling and Disposal of Chemicals. 7.D.3.3 Metal Azides. http://books.nap.edu/openbook.php?record_id=4911&page=165 (accessed March 11, 2011).

8. McMurry, J. *Organic Chemistry,* 7th ed.; Thompson: Belmont, CA, 2008; p 237, 624-625.

9. *Sodium Nitrite;* Material Safety and Data Sheet No. 563218; Sigma Aldrich: St. Louis, Missouri, (Feb 4) 2011, http://www.sigmaaldrich.com/catalog/DisplayMSDSContent.do (accessed March 11, 2011).

10. *Sodium Nitrate;* Material Safety and Data Sheet No. S5506; Sigma Aldrich: St. Louis, Missouri, (June 6) 2010, http://www.sigmaaldrich.com/catalog/DisplayMSDSContent.do (accessed March 11, 2011).

11. *Chromium Trioxide;* Material Safety and Data Sheet No. 27081; Sigma Aldrich: St. Louis, Missouri, (Mar 25) 2010, http://www.sigmaaldrich.com/catalog/DisplayMSDSContent.do (accessed March 11, 2011).

12. *Potassium Permanganate;* Material Safety and Data Sheet No. P2097; Sigma Aldrich: St. Louis, Missouri, (Dec 30) 2010, http://www.sigmaaldrich.com/catalog/DisplayMSDSContent.do (accessed March 11, 2011).

13. *Osmium Tetroxide;* Material Safety and Data Sheet No. O5500; Sigma Aldrich: St. Louis, Missouri, (Mar 13) 2010,

http://www.sigmaaldrich.com/catalog/DisplayMSDSContent.do (accessed March 11, 2011).

14. Ghanbari, H. Hot dog preservative could be disease cure. *USA Today* [Online] **2005**, http://www.usatoday.com/news/health/2005-09-05-hot-dog-drug_x.htm (accessed Mar 11, 2011).

15. Dawood, F. Template Directed Synthesis and Characterization of Nanocrystalline Metal Oxides and Chalcogenides. Ph. D. Thesis, Pennsylvania State University, State College, PA, May 2010.

16. Wang, Y.; Cai, L.; Xia, Y. *Adv. Mater*. **2005,** *17*, 473-477.

17. Brown, T.; LeMay, H.; Bursten, B. *Chemistry the Central Science,* 10th ed.; Pearson: Upper Saddle River; 2006; p 1128.

Chapter 4

Oxidation of In_3Sn to Indium Tin Oxide

4.1 Introduction

Tin-doped indium oxide (ITO) has received significant attention recently due to its unique properties such as optical transparency, electrical conductivity and its wide, tin dependent band-gap (1.38-4.14 eV).[1] These properties have yielded extensive applications in consumer electronics and as a transparent conducting layer in photovoltaic energy conversion.[2] In consumer products and solar cells, ITO is typically applied as a thin film. Traditional thin film deposition techniques include vacuum arc plasma evaporation, furnace evaporation/oxidation, magnetron sputtering, and molecular beam epitaxy.[3-6] Clearly, these methods are energy and cost intensive, requiring expensive apparati, and typically lead to significant product loss, which is non-trivial considering the current price of indium. An alternative synthetic and deposition method would be to utilize solution-mediated reactions to obtain the ITO nanoparticles, which could then be drop-casted as a thin film. Recent work has yielded solution-mediated ITO nanoparticle routes. These routes typically utilize the thermal decomposition of the In and Sn precursors in non-polar media, the alkaline hydrolysis of the In and Sn precursors, or the co-precipitation of the $In(OH)_3$ and $Sn(OH)_4$ to yield the ITO particles.[7-11]

Another route, of which there are few reports, is to synthesize either an In-Sn alloy[12] or possibly the β-In_3Sn intermetallic phase and thermally or chemically oxidize one of them to ITO, which is reported here. The synthesis is achieved by first generating the β-In_3Sn, made by the molten diffusion of In^0 into β-Sn particles, and then chemically oxidizing the β-In_3Sn to ITO using $NaNO_2$. There are several potential advantages to this method. One potential advantage is Sn variance of the ITO particles. The β-In_3Sn intermetallic phase has a natural variance of 12-44

% Sn. Thus, the subsequent oxidation of the β-In_3Sn nanoparticles would have a potential Sn:In ratio of 12-44 percent.[13] The Sn variability would affect the physical properties of the ITO nanoparticles: as the Sn content increases the band-gap would decrease and the electrical conductivity would increase. These relationships are due to Sn serving as the electron carrier in ITO. Another advantage is that the entire synthesis route can be accomplished at relatively low-temperatures, less than 180 °C. However, there are several challenges encountered using this synthetic route. The primary challenge is that In metal melts (m.p. = 157 °C) at a higher temperature than the β-In_3Sn (m.p. = 150 °C).[13] The eutectic lends the diffusion process to yield liquid particles. The liquid particles quickly combine with one another to produce larger particles and thus the shape and size control of the nanoparticles becomes difficult. Poor morphology control has been observed in other solution-mediated In-Sn alloy nanoparticle synthetic preparations.[14,15] Although addition of a surface stabilizer reduces the nanoparticle's surface-surface interactions, it still does not lead to facile shape and size control.

4.2 Experimental

4.2.1 Materials

The following materials were purchased and used without further purification: Polyvinylpyrrolidone (average m.w. = 55K, Alfa Aesar), $InCl_3$ (Alfa Aesar, 99.999%), $SnCl_2$ (Alfa Aesar, 99%), $NaBH_4$ (Alfa Aesar, 98%), Tetraethlyene glycol (TEG, Alfa Aesar, 99%), Trimethyl amine oxide dihydrate (TMAO, Alfa Aesar, 98%), Ethylene glycol (EG, Alfa Aesar, 99%), $NaNO_2$ (Alfa Aesar, 99%). All reactions were conducted in an air-free environment, in 3 necked flasks, and all work-ups were conducted at room temperature.

4.2.2 Synthesis

4.2.2.1 β-In_3Sn

PVP (55K, 0.400 g) was dissolved in 30 mL of TEG *via* stirring. $InCl_3$ (0.117 g) and $SnCl_2$ (0.044 g) were dissolved together in 10 mL TEG *via* sonication. $NaBH_4$ (0.337 g) was dissolved in 10 mL TEG *via* sonication. The PVP, $InCl_3$, and $SnCl_2$ solutions were combined, purged with Ar under continuous vigorous (800-1100 rpm) stirring. After the Ar purge, the $NaBH_4$ was injected drop wise over 2 min. Upon the injection, the reaction mixture turned black. The reaction mixture was then rapidly (~5 °C/min) heated to 180 °C and aged 40 min at 180 °C before being stopped. The reaction mixture was diluted 3:1 (ethanol: TEG) and centrifuged at 12000 rpm for 5 min. The collected particles were then re-suspended in ethanol and centrifuged at 12000 rpm for 4 min. The ethanol washes were conducted 3x and the particles were stored in ethanol.

4.2.2.2 β-In_3Sn to ITO using TMAO

One eighth of the pre-synthesized β-In_3Sn nanoparticles (~0.025 mmol, 0.0096 g) were suspended in 1.5 mL EG *via* sonication. The β-In_3Sn nanoparticles were added to 20 mL EG and purged with Ar under vigorous (800-1100 rpm) stirring. TMAO (0.209 g) dissolved in 3.5 mL EG was subsequently injected. The reaction mixture was rapidly (~5 °C/min) heated to 150 °C for 24 hrs before being stopped. The reaction mixture was diluted 3:1 (ethanol: EG) and centrifuged at 12000 rpm for 5 min. The collected nanoparticles were then re-suspended in ethanol and centrifuged at 12000 rpm for 4 min. The ethanol washes were conducted 3x and the particles were stored in ethanol. This procedure yielded ~5 % oxidation based on the powder XRD pattern.

To yield a higher % oxidation (~30 %), the same procedure can be followed above except after 2 hrs at 150 °C an additional injection of TMAO (0.116 g) should be added.

4.2.2.3 β-In_3Sn to ITO using $NaNO_2$

One eighth of the pre-synthesized β-In_3Sn nanoparticles were suspended in 1.5 mL EG *via* sonication. $NaNO_2$ (0.252 g) was dissolved in 8.5 mL EG *via* sonication. The suspended β-In_3Sn nanoparticles and $NaNO_2$ solution were combined with 10 mL EG and purged with Ar under continuous vigorous (800-1100 rpm) stirring. The reaction mixture was slowly (~1 °C/min) heated to 100 °C for 1 hr then the reaction temperature was slowly raised to 120 °C for 16 hrs before being stopped. The reaction mixture was diluted 3:1 (ethanol: EG) and centrifuged at 12000 rpm for 5 min. The collected nanoparticles were re-suspended in ethanol and centrifuged at 12000 rpm for 4 min. The ethanol washes were conducted 3x and the nanoparticles stored in ethanol.

4.2.3 Characterization

Powder XRD data were collected at room temperature using a Bruker D8 Advance Diffractometer with a LynxEye 1-D-detector (Cu Kα radiation). Transmission electron microscopy (TEM) images were obtained from a JEOL 1200 EX II operating at 80 kV. Scanning electron microscopy (SEM) images and energy-dispersive X-ray spectroscopy (EDS) data were obtained from a FEI Quanta 200 Environmental SEM operating in high vacuum mode.

4.3 Results and Discussion

As seen by the XRD patterns, the oxidation of β-In_3Sn to ITO (or some In_2O_3 and SnO_2 solid solution) was successfully completed using $NaNO_2$ and partially completed using TMAO.

The $NaNO_2$ oxidized the In_3Sn to ~90% oxide based on the powder XRD pattern, Figure 4-3. The remaining ~10% β-In_3Sn is likely in the center of the particle, considering the 50 nm diffusion barrier associated with the 100 nm β-In_3Sn nanoparticles. The reasons why the TMAO failed to completely oxidize the β-In_3Sn are low oxidizing potential and thermal degradation of the TMAO. TMAO is a milder oxidizing agent compared to $NaNO_2$; thus, it is less favored for it to oxidize the β-In_3Sn. Also, thermal degradation of the TMAO appears to have occurred because there was no difference in the percent oxidation after 24 hrs at 150 °C as oppose to 2 hrs at 150 °C. However, after a subsequent addition of TMAO at 150 °C the percent oxidation increased from ~5 % to ~30 %. The increase in oxidation is supporting evidence for thermal degradation of the TMAO.

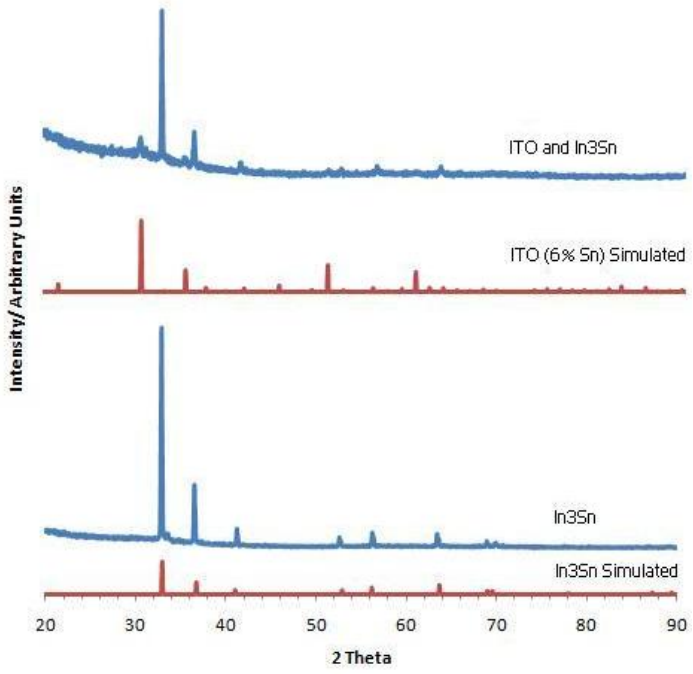

Figure 4-1: Powder XRD patterns of β-In_3Sn and the partially-oxidized product using a single injection of TMAO

As seen by the powder XRD patterns, the In_3Sn was marginally oxidized by the TMAO. The ITO peaks are considerably smaller than the β-In_3Sn peaks and it was estimated that the oxidation proceeded to ~5% completion.

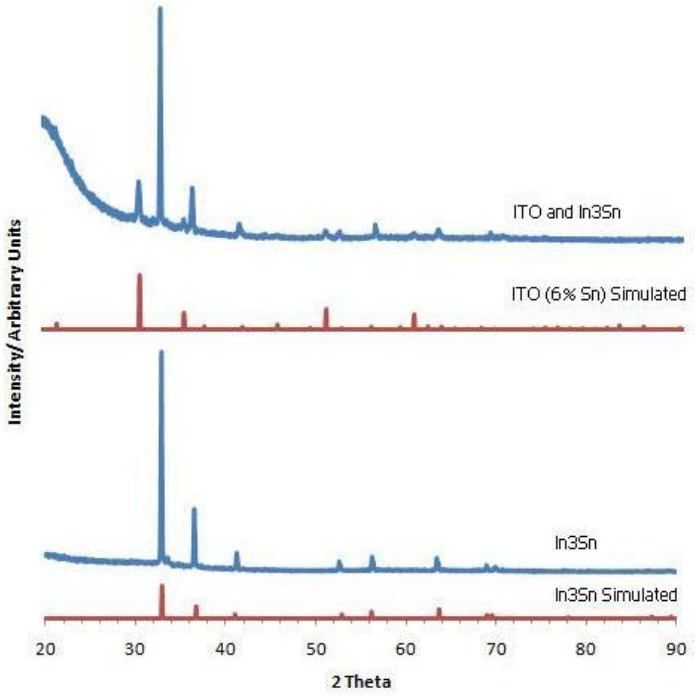

Figure 4-2: Powder XRD patterns of β-In_3Sn and the partially-oxidized product using a subsequent injection of TMAO

The powder XRD pattern of the subsequent injection of TMAO indicates that the additional TMAO further oxidized the β-In_3Sn. However, the further oxidation did not approach completion. Based on the XRD pattern, it can be estimated that the oxide product is ~20 % oxide.

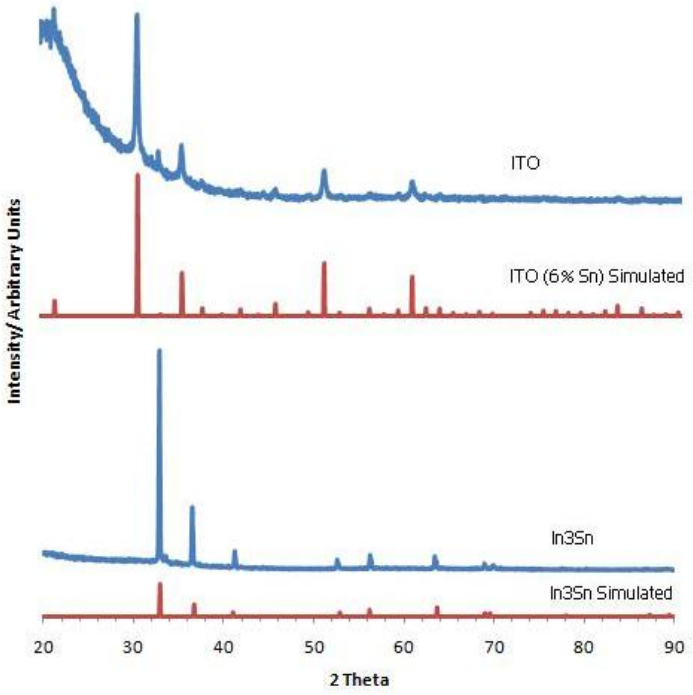

Figure 4-3: Powder XRD patterns of β-In_3Sn and the oxidized product using $NaNO_2$

As seen by the powder XRD pattern, the $NaNO_2$ successfully oxidized the β-In_3Sn to ITO with ~90 % completion. With a longer reaction time, it is likely that the $NaNO_2$ would have fully oxidized the β-In_3Sn to ITO. Also, if the In_3Sn nanoparticles were much smaller, then the diffusion distance would be less and the oxidation would likely have proceeded to further completion.

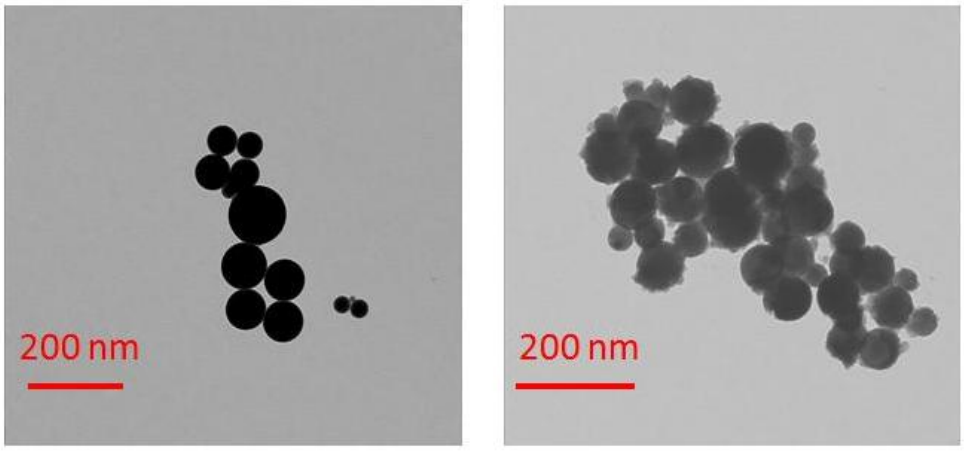

Figure 4-5: TEM images of β-In_3Sn nanoparticles (left) and ITO nanoparticles (right) synthesized using $NaNO_2$

As seen by the TEM images, the particle morphology was maintained during the oxidation process. Morphology preservation is important because for an oxidizing agent to have potential applications, the particle morphology must be maintained. As seen in the ITO TEM image (Figure 4-5), the spherical particles appear to have jagged growths off the nanoparticle surfaces. Theses jagged growths are consistent with oxide growth off of the nanoparticles, further confirmation of their oxidation.

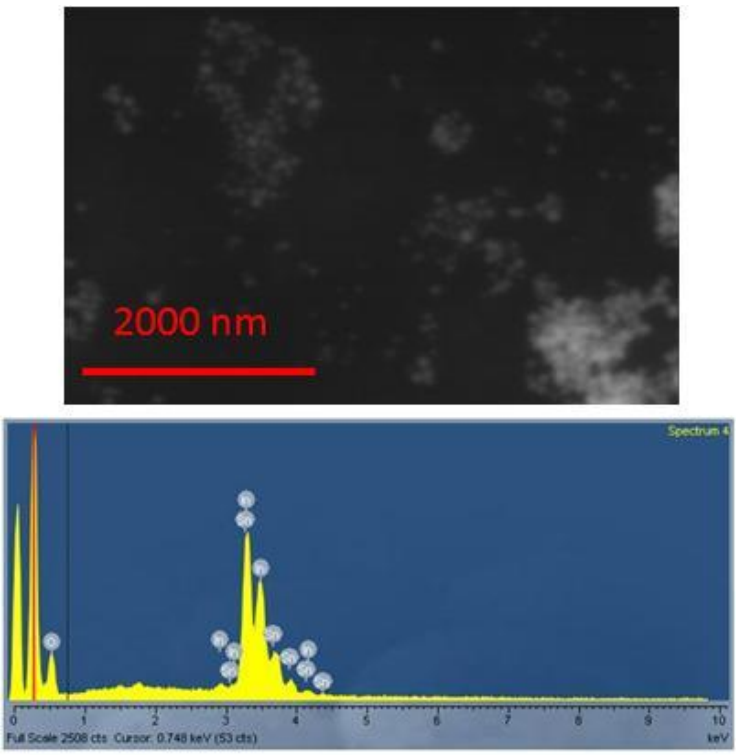

Figure 4-6: SEM image of ITO nanoparticles synthesized using $NaNO_2$ (top) and the EDS spectrum (bottom)

Element	Weight %	Atomic %
O	30.94*	76.47*
In	46.13	15.89
Sn	22.93	7.64

Table 4-1: Weight and atomic % obtained from the EDS of ITO nanoparticles synthesized using $NaNO_2$. *The oxygen weight and atomic percent is not consistent with ITO nanoparticles, but quantitative oxygen contents are not possible using this EDS system

As seen in the powder XRD patterns, the ITO synthesized matches the simulated ITO pattern which has 6 % Sn:In ratio. Considering that the β-In_3Sn, the precursor, contained ~25 atomic % Sn, it would appear as if the Sn leached out of the β-In_3Sn and formed the low percent

Sn content ITO phase. However, using the EDS on the SEM, it was confirmed that the surface (down to 55 Å, the tunneling distance of the SEM electrons) of the ITO particles contained 7.64 % Sn with an Sn:In ratio of 48 %. The EDS measurements represent the average X-ray energies from many of the nanoparticles surfaces. Using the particular instrument, it would have been impossible to accurately map the surface of one nanoparticle, since the particles were ~100 nm. The accuracy of the EDS measurements is also not ideal. Oxygen content cannot be accurately measured because oxygen is present on the SEM grid and thus the oxygen content will always be skewed. Also, the In and Sn contents may not be as precise as implied because In and Sn have significant overlap in the EDS spectrum. Nevertheless, the EDS measurements indicate that a significant amount of Sn remained on the surface of the ITO nanoparticles, which is not consistent with the Sn entirely leaching out of the nanoparticles.

The discrepancy between the powder XRD pattern and EDS measurements is likely due to an amorphous SnO_x and In_xO_y phase(s), which was likely present on the surface of the nanoparticles. This hypothesis implies that the core of the ITO nanoparticles is the low Sn content, crystalline phase and the surface is a different SnO_x and In_xO_y amorphous phase(s). Supporting this hypothesis is the EDS measurements because the EDS measurements confirmed that the surface of the ITO nanoparticles contained a 48 % Sn:In ratio. In sight of this, the jagged growths observed in the TEM image is likely the amorphous SnO_x and In_xO_y phase(s).

4.4 Conclusions

β-In_3Sn nanoparticles were successfully oxidized to ITO nanoparticles using $NaNO_2$ and partially oxidized to ITO using TMAO. The TMAO partially oxidized the β-In_3Sn due to its lower oxidation potential and thermal degradation of the TMAO. The particle morphology was

preserved during the oxidation process and jagged growths, presumed to be oxide growth, were observed on the surface of the ITO nanoparticles. Although the powder XRD patterns indicate the synthesis of a low Sn content ITO phase, EDS measurements indicated the preservation of the Sn by a 48% Sn:In ratio. Since EDS is a surface characterization technique, the observed jagged growths are likely an amorphous SnO_x and In_xO_y phase(s).

4.5 References

1. Gupta, L.; Mansingh, A.; Srivastava, P. *Thin Solid Films* **1989,** *176,* 33-44.
2. Kim, K.; Park, S. *Mater. Chem. Phys.* **2004,** *86,* 210-221.
3. Minami, T.; Ida, S.; Miyata, T. *Thin Solid Films* **2002,** *416,* 92-96.
4. Balasubramanian, N.; Subrahmanyam, A. *J. Phys. D: Appl. Phys.* **1989,** *22,* 206-209.
5. Meng, L.; dos Santo, M. *Thin Solid Films* **1998,** *322,* 56-62.
6. Dwyer, C.; Szachowicz, M.; Visimberga, g.; Lavayen, V.; Newcomb, S.; Sotomayor Torres, M. *Natr. Nanotechnol.* **2009,** *4,* 239-244.
7. Kim, H.; Kim, M.; Ha, Y.; Kanatizids, M.; Marks, T.; Facchetti, A. *J. Am. Chem. Soc.* **2009,** *131,* 10826-10827.
8. Park, Y.; Seo, K.; Lee, J.; Kim, J.; Cho, S.; O'Conner, C.; Lee, J. *J. Electroceramics* **2004,** *13,* 851-855.
9. Paramanik, N.; Biswas, P. *Bull. Mater. Sci.* **2002,** *6,* 505-507.
10. Saski, T.; Endo, Y.; Nakaya, M.; Kanie, K.; Nagatomi, A.; Tanoue, K.; Nakamura, R.; Muramatsu, A. *J. Mater. Chem.* **2010,** *20,* 8153-8157.
11. Kanehara, M.; Koike, H.; Yoshinaga, T.; Teranishi, T. *J. Am. Chem. Soc.* **2009,** *131,* 17736-17737.
12. Zhenguo, C.; Wang, C.; Zhao, L.; Zhou, Q. *Mater. Lett.* **2006,** *60,* 3096-3099.
13. *Phase Diagrams for Binary Alloys.* Okamoto, H.; ASM International: Materials Park, OH, 2000; p 491.
14. Zhao, Y.; Zhang, Z.; Dang, H. *J. Mater. Chem.* **2004,** *14,* 299-302.

15. Jiang, H.; Moon, K.; Sun, Y.; Wong, C.; Hua, F.; Pal, T.; Pal, A. *J. Nanopart. Res.* **2008,** *10*, 41-46.

VITA

MATTHEW D. STRAESSER

EDUCATION

The Pennsylvania State University, University Park, PA

- Bachelor of Science in Chemistry, expected May 2011 2007-present
- Schreyer Honors College
- Scholar of Distinction

HONORS AND AWARDS

- Fleming-Meyer Analytical Award, 2010
- Teas Summer Research Fellowship, 2010
- Teas Science Scholarship, 2009
- Eagle Scout, 2004

PUBLICATION

Henderson, Nathaniel L.; Straesser, Matthew D.; Sabato, Philip E.; Schaak, Raymond E. Towards Green Metallurgy: Low-Temperature Solution Synthesis of Bulk-Scale Intermetallic Compounds in Edible Plant and Seed Oils. *Green Chem.* **2009,** *11,* 974-978.

RESEARCH EXPERIENCE

Research Assistant, Penn State University May 2009-present

- Research Advisor, Assoc. Prof. Raymond Schaak
- Interdisciplinary research in nanochemistry: nanoparticle synthesis and materials chemistry
- Instrumental Use: Powder XRD, TEM, SEM, DSC, UV-Vis